DISTRIBUTION STATEMENT A. Approved for public release; distribution is unlimited.

Dynamic Camouflage in Benthic and Pelagic Cephalopods: An Interdisciplinary Approach to Crypsis Based on Color, Reflection, and Bioluminescence

Sönke Johnsen
Biology Department, Duke University
Durham, NC 27708
phone: (919) 660-7321 fax: (919) 660-7293 email: sjohnsen@duke.edu

Alison Sweeney
Physics and Astronomy Department, U. of Pennsylvania
Philadelphia, PA 19104
phone: (215) 573-7569 fax: (215) 898-2010 email: alisonsw@physics.upenn.edu

Daniel Morse
Marine Science Institute, U. of California at Santa Barbara
Santa Barbara, CA 93106
phone: (805) 893-8982 fax: (805) 893-7998 email: d_morse@lifesci.ucsb.edu

Dariusz Stramski
Marine Physical Lab, Scripps Inst. of Oceanography, UCSD
La Jolla, CA 92093
phone: (858) 534-3353 fax: (858) 534-7641 email: dstramski@ucsd.edu

Jules Jaffe
Marine Physical Lab, Scripps Inst. of Oceanography, UCSD
La Jolla, CA 92093
phone (858) 534-6101 fax: (858) 534-7641 email: jules@mpl.ucsd.edu

Award Number: N00014-09-1-1053
http://www.biology.duke.edu/johnsenlab

LONG-TERM GOALS

Our overall goal is to understand the perceptual and mechanistic principles that underlay camouflage framed in the context of the animals' environment. In particular, we hope to characterize and understand the perceptual abilities of several species of benthic and pelagic cephalopods, the aspects of their optical environment that affect their camouflage behavior, the characterization of that behavior, and the molecular mechanisms inside the skin by which those responses are accomplished.

OBJECTIVES

1. To characterize the spatiotemporal characteristics of the near-surface and shallow benthic underwater light field, including ultraviolet radiation and polarization.

2. To determine the visual abilities of several species of cephalopod and model both the shallow and deep-water world from the animals' points of view.

3. To incorporate the knowledge gained from objectives 1 and 2 in order to study the camouflage behavior of these species under simulated ocean conditions.

4. To understand the underlying molecular and biophysical mechanisms governing changes in the skin that produce the observed optical effects, to provide a platform for future translational efforts.

APPROACH

Objective 1, Light measurements: Our approach to characterize the underwater light fields includes radiometric measurements with custom-built SQUID and Porcupine instruments and commercial hyperspectral sensors from TriOS(Germany) and Satlantic (Canada). SQUID (SeQuence of Underwater Irradiance Detectors) was developed for this project to provide a unique capability to measure both spatial and temporal statistical properties of downwelling irradiance fluctuations produced by surface-wave focusing within the surface ocean layer. The Underwater Porcupine Radiometer System was developed for the ONR RaDyO program to measure temporal properties of high-frequency fluctuations in downwelling radiance and irradiance at several light wavelengths, and it complements SQUID measurements in this project. Both SQUID and Porcupine provide light measurements with a high sampling rate of 1 kHz. The TriOS and Satlantic sensors provide measurements of irradiance and radiance with an averaging time typically from about 0.002 to >1 s (depending on light intensity) and with high spectral resolution (~3 nm from 350 to 850 nm). Radiative transfer simulations are also used in this project as an additional tool to characterize the underwater light field.

Deep-sea light measurements: As part of this MURI the Jaffe Lab also created two in situ sensors for measuring light in the ocean. In one case the Omni-Cam instrument was reconfigured to maximize sensitivity for deep-sea ambient light measurements [Jaffe et al., 2011]. In the other case, an entirely new very sensitive deep-sea radiometer was built and bi-spectral light measurements were recorded [Haag et al, 2014], very interestingly verifying the computational work of Li et. al [2014].

***Objective 2, visual physiology*:** our approach involved using various techniques to measure the visual parameters of various study species, including field of view, spectral sensitivity, acuity, temporal resolution, and contrast and polarization sensitivity. Field of view was determined from the placement and orientation of the eyes and the geometry of the retina and pupil. Spectral sensitivity was investigated using microspectrophotometry (MSP), which measures the absorption spectra of individual photoreceptors. Spatial and temporal resolution will be estimated fro m the spacing of photoreceptors in the retina and the optical quality of the lens. Polarization sensitivity was assayed via retinal morphology and behavioral response.

Objective 3, camouflage behavior: *Sepia officinalis* camouflage behavior was studied using a "holodeck", a tank surrounded by monitors that project natural environments or controlled visual

stimuli. We also studied the basic principles octopuses use to camouflage by investigating substrate choice and resulting body pattern use. When we placed *Octopus bimaculoides* on colored pebbles, the animal changed its overall body color and patterns according to the shading and distribution of the pebbles. We also investigated how the body patterns used by the cuttlefish *Sepia officinalis* change over time and with repeated exposure to a range of backgrounds. We also used the holodeck to present animated footage of brief squid (*Lolliguncula brevis*) color change during attack, and video captured prey response. We recorded actual attacks from flamboyant cuttlefish (*Metasepia pfefferi*) on mysids to measure color change variation and attack success. We presented cuttlefish (*Sepia officinalis*) with controlled environments to determine their camouflage reaction to environmental features placed at variable distances from the subject. We analyzed controlled behavioral trials of *L. brevis* to assess the function of conspicuous signaling that females use to break camouflage in mating situations. Additionally, we synthesized literature reviews of perception and behavior to make predictions related to camouflage behaviors.

Bioelectric crypsis: Behavioral and electrophysiological responses of cuttlefish were studied in live cuttlefish presented with a video of a looming predator on a screen positioned outside of the tank. Resting parameters for body movement (amplitude and frequency) and bioelectric potentials (amplitude and frequency) were quantified during the pre-stimulus portion of each video. Response parameters (amplitude and frequency for both body movements and bioelectric potentials) were quantified during the looming predator stimulus portion of each video. Body movements were continuously recorded with video cameras positioned in front of and above the cuttlefish inside an experimental tank. Bioelectric potentials were continuously recorded from a glass recording electrode positioned near the gills (Figure 1). Behavioral responses were recorded from two shark species that use electroreception to detect bioelectric fields for prey capture.

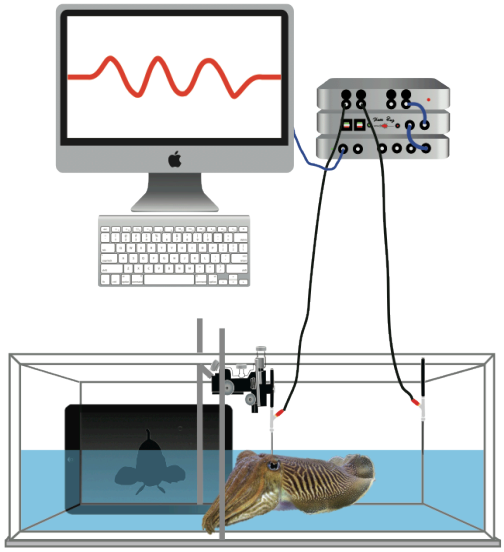

Figure 1: Experimental set-up for recording behavioral and physiological responses of cuttlefish,* Sepia officinalis*, to a looming predator stimulus. (a) A video of a looming fish predator was played on an iPad positioned along one wall of an experimental tank. Behavior (body movement from ventilation) and bioelectric field responses (associated with ion exchange during ventilation) were recorded over the course of the predator simulation with video cameras and a recording electrode positioned at the opening of the mantle.

Toxicology: Identification and quantification of tetrodotoxin (TTX) in tissues collected from two cuttlefish species, one which exhibits background matching camouflage (*Sepia bandensis*), and one which exhibits conspicuous coloration (*Metasepia pfefferi*), were completed using high-performance liquid chromatography with fluorescence detection (HPLC-FLD) and competitive inhibition enzyme immunoassays (CIEIA). CIEIA enables quantification of tetrodotoxin extracted from cuttlefish tissues, while HPLC verifies identification of TTX and its potential analogs found in tissue samples.

Kinematics: To quantify kinematic and morphometric variables associated with feeding tentacles used for prey capture by cuttlefish, a high speed video camera was used to record prey capture events from cuttlefish in an experimental tank. Because cuttlefish strike behaviors are likely linked to cuttlefish species and prey type, we filmed two species of cuttlefish which use similar feeding behaviors, but which exhibit differences in morphometrics of the feeding tentacles. *Sepia bandensis* has shorter, but larger diameter feeding tentacles, indicating that strikes are initiated at a closer distance with a potentially lower velocity. Conversely, *Metasepia pfefferi* have comparatively longer and narrower diameter feeding tentacles, which may allow strike initiation at a longer distance, resulting in a higher velocity.

Objective 4, biophotonics: We characterized the optics of the skin using fiber-optic spectroscopy coupled with goniometry, measuring the polarization-specific bidirectional reflectance of the skin of the target species and correlated these with light measurements from objective 1 to determine which aspects of this complex reflectance have specifically evolved for camouflage. We also determined the ultrastructure of the reflectin-based structures using transmission electron microscopy and model their optical effects to determine what aspects of the biological structures are important for the observed environmental optical match. Finally, we also investigated the biophysical mechanisms governing tunable, self-assembling reflectance.

WORK COMPLETED

Objective 1, Light measurements: The Stramski team from SIO developed the SQUID (SeQuence of Underwater Irradiance Detectors) instrument, which was designed and fabricated specially for this project. The SQUID consists of 25 irradiance sensors, which are positioned at different distances from one another along a 2.5 m long linear array (Figure 2). The array of sensors can be oriented at any desired direction (e.g., predominant wind/wave direction or solar principal plane) when the instrument is deployed on the seafloor. The SQUID measures downward plane irradiance E_d at a selected light wavelength (typically 532 nm) with a high sampling rate of 1 kHz using a cosine collector of very small size (2.5 mm in diameter). The SQUID provides a unique capability to measure spatiotemporal statistical properties of irradiance fluctuations produced by surface-wave focusing within the near-surface ocean layer. The SQUID was deployed during the field experiment in Santa Catalina Island in September-October 2011 (Figure 3). We collected a unique data set consisting of 140 time-series of light fluctuations, each with 10 min duration. The SQUID measurements were accompanied by measurements taken with Porcupine instrument and other optical instruments.

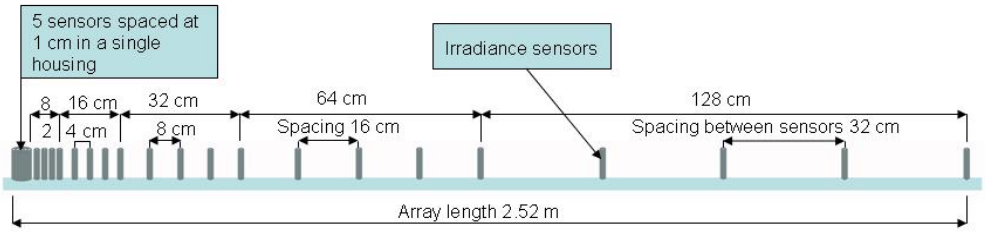

Figure 2: Schematic diagram of SQUID.

Figure 3: Deployment of SQUID during Santa Catalina experiment.

The Stramski team also participated in three project-sponsored cruises. Two cruises were in the Gulf of California on R/V New Horizon in 2010 and 2011. The third cruise was in the Pacific waters off Hawaii Islands on R/V Kilo Moana in 2012. The main task on the cruises was to measure the vertical profiles of underwater light field with the TriOS or Satlantic hyperspectral systems. These measurements were typically made in a vertical profiling mode from the surface to depths as large as 150 m at different times of the day to cover a broad range of solar zenith angles and environmental conditions. Some deployments were made with the optical sensors oriented horizontally to study the asymmetry of horizontal radiance within the upper ocean. Ancillary measurements and analyses were also made to characterize the inherent optical properties and optically significant constituents of seawater, for example the spectral absorption coefficient, phytoplankton pigment concentration, particulate organic carbon concentration, and mass concentration of suspended particulate matter.

The analysis of power spectra of wave-induced light fluctuations at near-surface depths in the ocean under sunny conditions based on data collected with SQUID and Porcupine instruments was completed (Sawicka et al., 2012). This work represents a chapter of PhD thesis of E. Gassmann and the manuscript is in preparation for publication (Gassmann et al., in prep). The analysis of horizontal radiance data collected during the cruise of Hawaii was completed. This analysis was supplemented by radiative transfer simulations. This study also contributes to the PhD thesis of E. Gassmann and is being prepared for publication (Gassmann et al., in prep). The work on the asymmetry of horizontal radiance also resulted in a collaborative paper (Johnsen et al., 2014). The analysis of data collected in the Gulf of California was completed. This analysis focused on distinctive features of underwater light field associated with the effects of inelastic radiative processes and was also supplemented by radiative transfer simulations. This study contributes to the PhD thesis of L. Li and is in preparation for

publication (Li et al., in prep). A comprehensive study of the solar light field within the ocean mesopelagic zone based on a large set of radiative transfer simulations was completed and published (Li et al., 2014). In the context of the characterization of deep sea light field the Stramski team also contributed to a collaborative paper (Haag et al., 2014).

The Omnicam instrument was configured to maximize sensitivity for deep-sea ambient light measurements. By reconfiguring the camera parameters, it was possible to increase low light sensitivity. Although the captured images had decreased resolution, this allowed for ambient light to be measured deeper than previously possible. Tests were performed off SIO pier and field deployments were on *R/V New Horizon* (Figure 4). Based on the field study results, it was decided that more sensitive detectors would be needed. As such, a comparative analysis of highly sensitive detectors was performed and it was decided that, adequate technology was available to obtain extremely low light level observations by fabricating a new instrument.

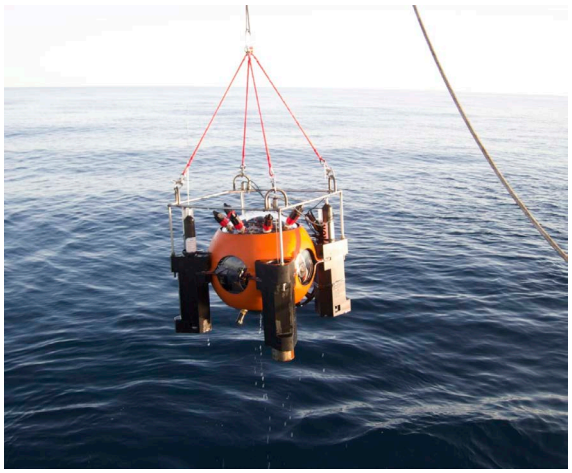

Figure 4: Omnicam deep-sea configuration during New Horizon deployments.

We therefore created a deep-sea radiometer using the latest technology that consisted of solid state PMTs. Two single-waveband low-light radiometers were developed to characterize properties of the underwater light field relevant to biological camouflage at mesopelagic ocean depths. Phenomena of interest were vertical changes in downward irradiance of ambient light at wavelengths near 470 nm and 560 nm, and flashes from bioluminescent organisms. Depth profiles were acquired at multiple deep stations in different both the Atlantic and Pacific.

Objectives 2 and 3, visual physiology and camouflage behavior: Many cephalopods change color while they attack prey. We are investigating the possibility that this color change confuses prey, acting to camouflage attack motion. We assessed how brief squid, *Lolliguncula brevis,* change color through time points 1, 2, and 3 of an attack (figure 5B), and tested whether this sequence changes prey escape response relative to controls with no color change (figure 5A and 5C). We presented animated squid attack to *Palaemonetes* (shrimp) and *Poecilia latipinna* (Sailfin molly fish). We also assessed color change attack strategies in *Metasepia pfefferi* (flambouyant cuttlefish) that were targeting mysid shrimp (Order Mysida) and conducted trials to determine whether color change strategy influenced attack success.

We collected preliminary data for behavioral studies of cuttlefish camouflage strategies. We plan to define the elicitation space for camouflage patterns, or the spatial area over which environmental stimuli influence camouflage response (Figure 6). This initial work attempts to assess the elicitation space for very basic camouflage pattern components responding to simple environmental stimuli. It also explores whether camouflage strategies respond to spatial and temporal abundance of features in the environment, by testing whether cuttlefish preferentially match common rather than rare objects in the environment.

We also conducted a comprehensive review of the role of proportion-based perception in animals and how this is predicted to influence the evolution of behaviors and sensory scene analysis. This work identifies several trends in behavioral evolution that lead to specific predictions about camouflaged behavior. We also applied this theory to explore the evolution of conspicuous behaviors in an invited chapter for a book about perception and cognition in animal communication (Akre and Johnsen, 2014).

We also analyzed video trials of *L. brevis* to investigate the unique visual signaling system of squid that live in a turbid marine environment. Females of this species produce more sexual signals than males do, in spite of living in estuarine waters with low visibility. Visual signaling is normally less elaborate in low visibility conditions, and these squid break their clear skin camouflage when producing chromatophore signals. We analyzed female and male interactions to investigate how these squid use their mating signals (ethogram presented in figure 7; Akre et al. in prep).

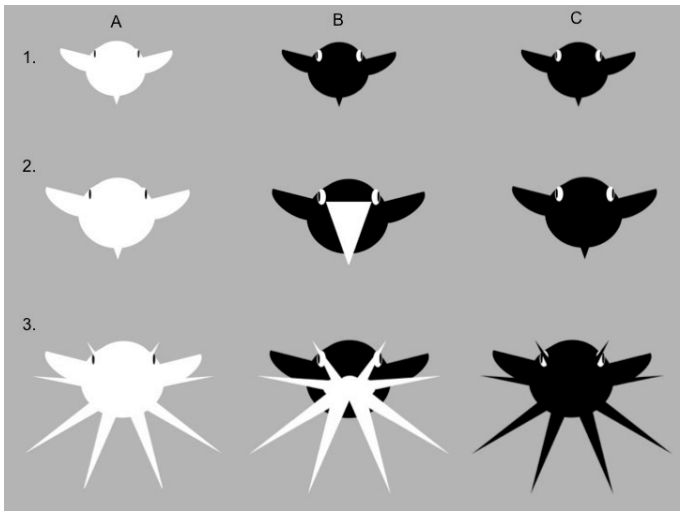

Figure 5: Some cephalopods change color during attack. Column B shows sequence of color change during* Lolliguncula brevis *attack through time points 1, 2, and 3. Controls are shown in columns A and C.

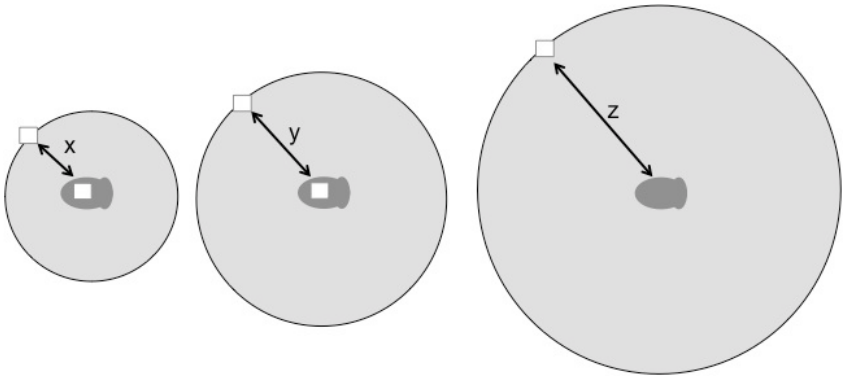

Figure 6: Camouflage patterns are elicited by environmental features. To determine the elicitation distance for the white square component of this cuttlefish pattern, we can measure the distance from which a white rock elicits the pattern. Here, y < elicitation distance < z.

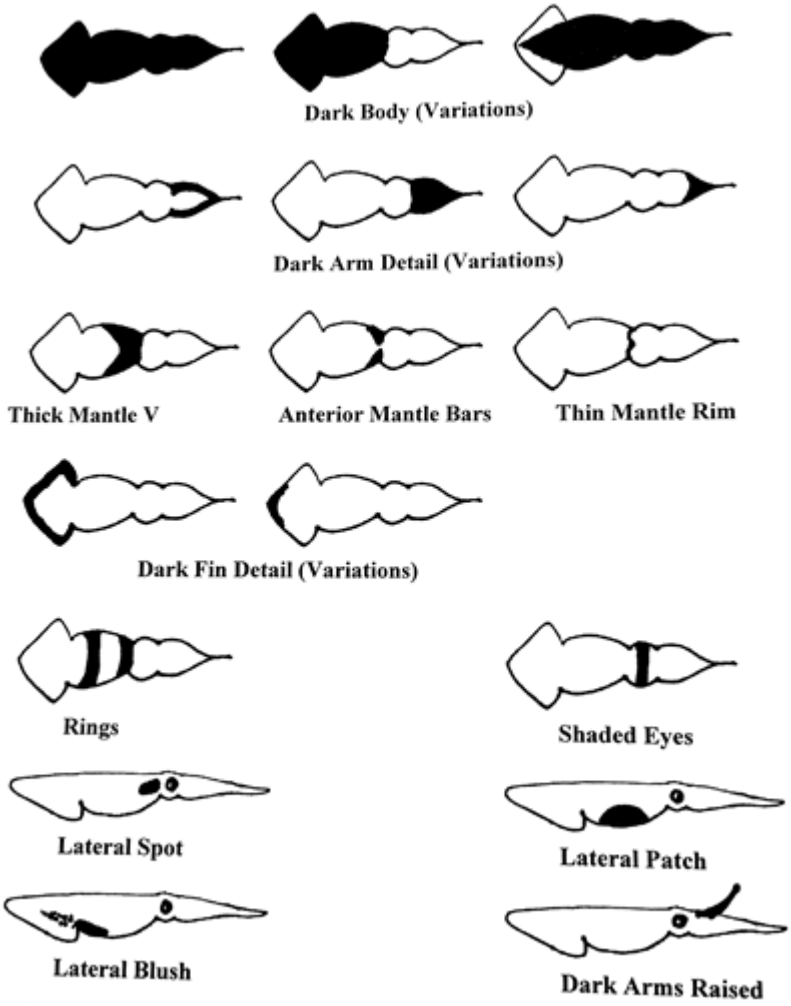

***Figure 7: Ethogram of most common chromatophore signals produced by* L. brevis.**

Bioelectric crypsis: Body movements and bioelectric potentials were recorded from eight cuttlefish (*Sepia officinalis*). Body movements and ion exchange at the gills in cuttlefish, *Sepia officinalis*, are associated with ventilation and act as both visual (motion) and electric stimuli for electrosensitive predators. The signals are modulated to decrease detection by predators in response to a predator-simulating stimulus. Motion and bioelectric stimuli were recorded from *S. officinalis* in response to a looming fish predator stimulus (Figure 1). The DC electric stimuli recorded from *S. officinalis* during rest, freeze (predator-avoidance response), and jet (escape) behaviors were used in a behavioral assay to quantify bonnethead shark, *Sphyrna tiburo*, and blacktip shark, *Carcharhinus limbatus*, responses to electric fields associated with these different behaviors.

Cuttlefish toxicology: Bright body coloration, such as that of the flamboyant cuttlefish (*Metasepia pfefferi*), is often associated with toxic animals and is thought to function as a warning of toxicity to potential predators. Almost all other species of cuttlefish, such as those of the genus *Sepia,* match their background substrate and are more subtly colored in order to provide camouflage. To determine if the conspicuousness is correlated to toxicity in cuttlefish, we compared concentrations of the most common marine animal toxin, tetrodotoxin (TTX), in tissues collected from *Metasepia* and *Sepia* cuttlefish. Digestive, reproductive, cardiac, respiratory, ink, and skin tissue samples were collected from expired cuttlefish. Samples were first surveyed using a competitive inhibition binding enzyme immunoassay (CIEIA) to determine 1. if TTX is present in any tissue and 2. the concentration of toxin in the TTX^+ tissues. TTX^+ tissues were then analyzed via high-performance liquid chromatography fitted with a fluorescence detector (HPLC-FLD) to confirm that TTX is present in those tissues and determine if the TTX^+ tissues contain either pure TTX or an analog of the toxin. All CIEIAs have been completed and HPLC-FLD has been completed on a small subset of TTX^+ tissues.

Cuttlefish feeding kinematics: Feeding events from two species of cuttlefish (*Metaspia pffeferi* and *Sepia bandensis*), which exhibit differences in the gross morphology of their feeding appendages were recorded using a Photron APX-RS high speed video camera. A total of 130 feeding events were recorded at 1000-3000fps from eight *Metasepia* and seven *Sepia*. All feeding sequences have been digitized by placing markers on the feeding tentacles and head of the cuttlefish, as well as the head of the shrimp or fish prey in order to track the predator and prey movement through the event. The maximum of extension of the feeding tentacles has been calculated from all videos resulting in a successful strike and the maximum velocity, acceleration, and power were calculated from the successful strike sequences recorded at 2000fps or faster. All sequences are currently being analyzed to provide a description of the behaviors as they progress through feeding stages that have been described in previous literature. To determine how morphology and behavior may be conserved across taxonomic groups, cuttlefish behavior and kinematics are being compared to another cephalopod, the squid *Loligo peali* (studied by Kier and van Leeuwen, 1997) that uses feeding tentacles for prey capture, as well as chameleons of the genus *Chameleo* that use some of the fastest protrusible ballistic-style feeding appendages of any animal.

Objective 4, biophotonics and instrumentation development: We completed our elucidation of the ultrastructural basis and unifying biophysical mechanism controlling the dynamically tunable "structural color" and the switchable, omnidirectional white produced by the reflective iridocytes and leucophores in cephalopod skin. In addition to discovering the unification of the underlying mechanism of these two dynamically controllable biophotonic systems, our work provides new insights into the principles of camouflage for moving objects and edge-disruption in "caustic" light environments.

RESULTS

Objective 1, Light measurements: With regard to the studies on the characterization of underwater light field which were conducted by the Stramski team from SIO, in this report we present some unique example results of wave-induced light fluctuations at near-surface depths from measurements with SQUID instrument as well as results from radiative transfer simulations of mesopelagic light field. Figure 8 shows that wave focusing can produce instantaneous values of irradiance which exceed the time-average irradiance more than 30-fold at shallow depths of about 1 m under sunny conditions. To our knowledge, the occurrence of such high concentrations of solar energy in natural aquatic environments has never been demonstrated before. Figure 9 shows measurements taken with 1 kHz sampling rate during a 1 s period simultaneously with eleven SQUID sensors positioned at different locations along a linear array of the instrument. This graph shows a unique capability of SQUID to provide spatial and temporal information about wave-induced light fluctuations at time scales as short as milliseconds and spatial scales as small as centimeters. This capability is essential for resolving spatial and temporal scales of wave-induced light fluctuations at shallow depths under sunny conditions. We see, for example, that a propagation of a specific focusing event, whose duration at a given point in space is on the order of tens of milliseconds, is observed over a distance > 20 cm. Figure 10 compares the spatial autocorrelation functions of downward irradiance for weak (1.8 m s^{-1}) and moderate (7.2 m s^{-1}) wind conditions. These results indicate that the spatial decorrelation scale is significantly smaller under weak winds when light fluctuations are very strong, compared with higher wind speeds when the fluctuations are weaker. A decrease in the intensity of irradiance fluctuations with increasing wind speed is illustrated in Figure 11. This figure shows a significant reduction in the magnitude of power spectra of irradiance fluctuations at a wind speed of 7.2 m s^{-1} compared with the wind speed of 1.8 m s^{-1}. In addition, the damping of high-frequency (> 2 Hz) content of fluctuations is more pronounced when the winds are stronger. These results are consistent with the interpretation that an increased roughness of the sea surface at high winds is significantly less efficient in producing focusing events than sea surface waves under weak winds.

The quantitative knowledge of the solar light field within the mesopelagic zone (depth range 200 - 1000 m) has been very limited, so our study makes a breakthrough advancement in this scientific area. We performed radiative transfer simulations of solar light field within the entire water column down to 1000 m. The simulations were made for several scenarios of surface boundary conditions and inherent optical properties within the ocean surface layer which provided, for the first time, a comprehensive characterization of variations in the magnitude, spectral composition, and angular distribution of various radiometric quantities of the solar light field as well as the behavior of apparent optical properties (AOPs) within the entire mesopelagic zone across the entire visible spectrum of light. Figure 12 illustrates a very large dynamic range of irradiance within the mesopelagic zone as well as the dominant contribution of inelastic radiative processes to the mesopelagic light at wavelengths longer than 500 nm. The spectral values of scalar irradiance decrease typically by about 9-10 orders of magnitude between the top and bottom of the mesopelagic zone. Ignoring the presence of inelastic processes in the ocean yields totally unrealistic results in the green and red portions of the spectrum but has small or negligible effect in the blue. Raman scattering by water molecules plays the most important role among the inelastic processes but the effects of fluorescence of CDOM at mesopelagic depths are also significant. Figure 13 shows that the angular distribution of mesopelagic light is dramatically different at different light wavelengths. In the blue, the radiance distribution at mesopelagic depths all the way down to 1000 m is dominated by downwelling light. In contrast, in the red the radiance distribution is nearly uniform, which is caused by the contributions of inelastic processes. A closer inspection of such radiance data reveals that the shape of the angular distribution of

light remains nearly unchanged throughout the deeper portion of the mesopelagic zone (below approximately 400 - 500 m), implying that the light field reached the asymptotic regime. The results for the AOPs support this conclusion. Figure 14 shows spectra of three example AOPs, the average cosine of total light field, diffuse attenuation coefficient of downward plane irradiance, and irradiance reflectance. For all three cases the spectra of these AOPs converge on one another for the example mesopelagic depths of 500, 800, and 1000 m. This comprehensive characterization of the mesopelagic light field accomplished through radiative transfer simulations is expected to benefit studies of vision and crypsis of mesopelagic animals and serve as a reference for interpretation of deep-sea light measurements.

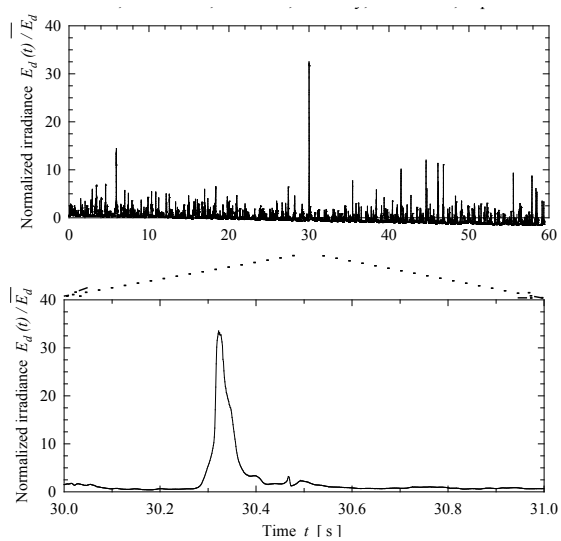

Figure 8: Example 1-min and 1-s time-series of fluctuations in downward irradiance at 532 nm measured at a depth of 1.16 m during the Catalina experiment under clear skies and weak wind. The downward irradiance is normalized by the time-average value of irradiance.

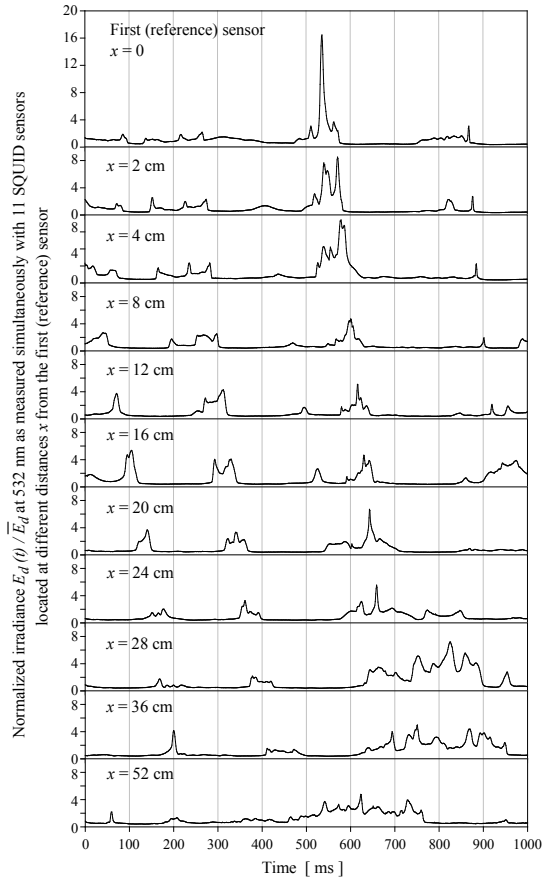

Figure 9: Example 1-s time-series of fluctuations in downward irradiance at 532 nm measured simultaneously with eleven SQUID sensors at a depth of 1.16 m during the Catalina experiment under clear skies and weak wind. The distance, x, between the sensors along a linear array is indicated.

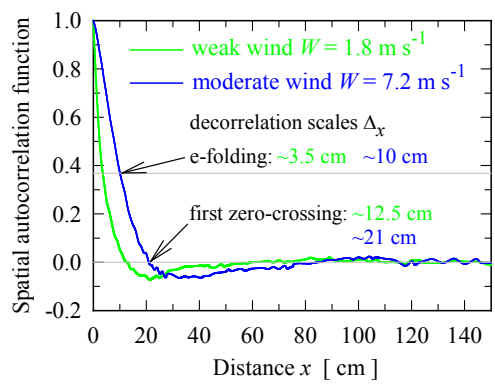

Figure 10: Spatial autocorrelation functions of fluctuations in downward irradiance at 532 nm for weak and moderate wind conditions. The functions were computed from measurements with SQUID taken at a depth of 1.16 m during the Catalina experiment under clear skies.

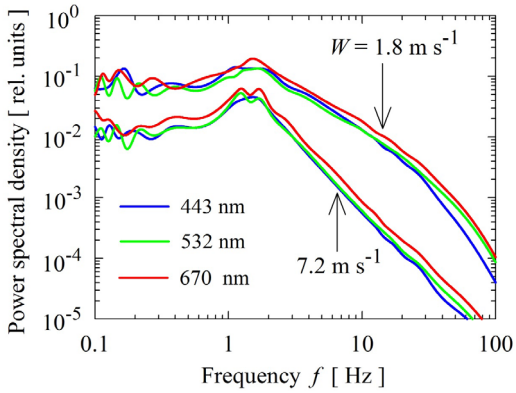

Figure 11: Power spectra of fluctuations in downward irradiance at three light wavelengths (443, 532, and 670 nm) for weak and moderate wind conditions. The measurements were taken at a depth of 1.16 m during the Catalina experiment under clear skies.

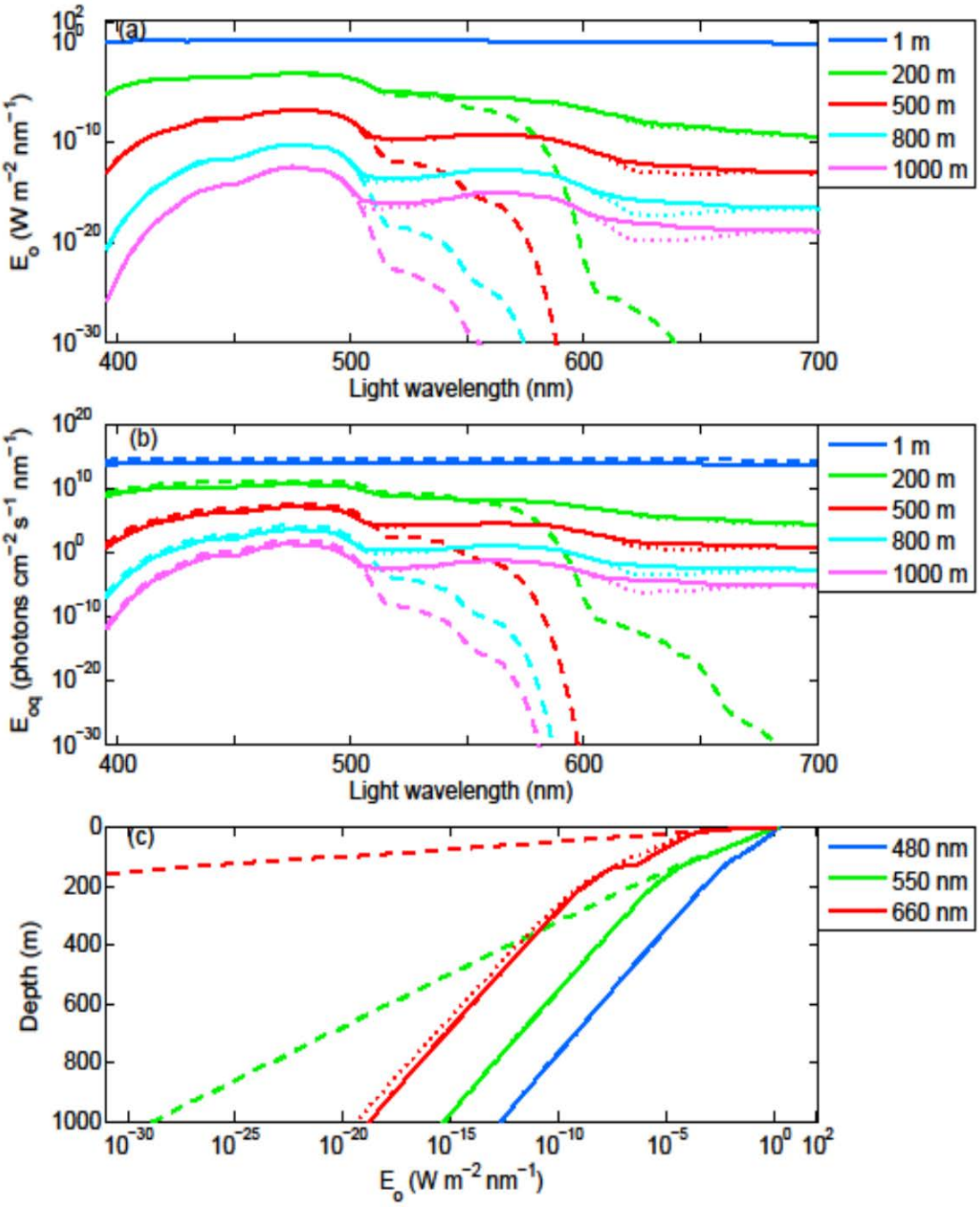

Figure 12 (a): Spectra of scalar irradiance E_o for selected depths as indicated; (b): Spectra of quantum scalar irradiance E_{oq} derived from E_o presented in panel (a); (c): Depth profiles of E_o for selected light wavelengths as indicated. Dashed lines represent radiative transfer simulations with no inelastic radiative processes; dotted lines represent simulations with Raman scattering by water molecules included; and dashed lines represent simulations with Raman scattering and fluorescence of CDOM and chlorophyll-a included. These results were obtained for clear sky conditions with solar zenith angle of 30° and the chlorophyll-a concentration in the surface layer Chl = 0.2 mg m^{-3}.

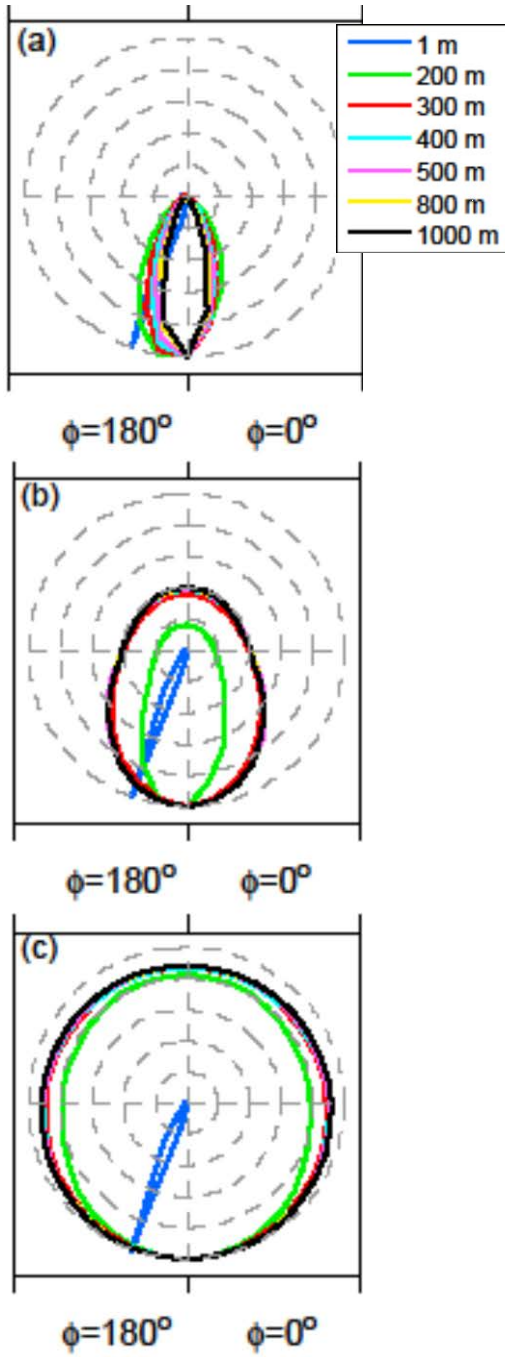

Figure 13: Diagrams illustrating the shape of the angular distribution of radiance at three selected wavelengths, 480 nm (panel a), 550 nm (panel b), and 660 nm (panel c) for selected depths as indicated. To facilitate a comparison of shapes the radiance values of each distribution were normalized by the maximum value of radiance. The distributions are within the solar principal plane. The right half of the plane denoted as $\phi = 0^o$ contains the sun. The left half of the plane denoted as $\phi = 180^o$ is the opposite part of the solar principal plane. These results were obtained from simulations for clear sky conditions, solar zenith angle of 30°, and the chlorophyll-a concentration in the surface layer Chl = 0.2 mg m^{-3}. The inelastic radiative processes were included in the simulations.

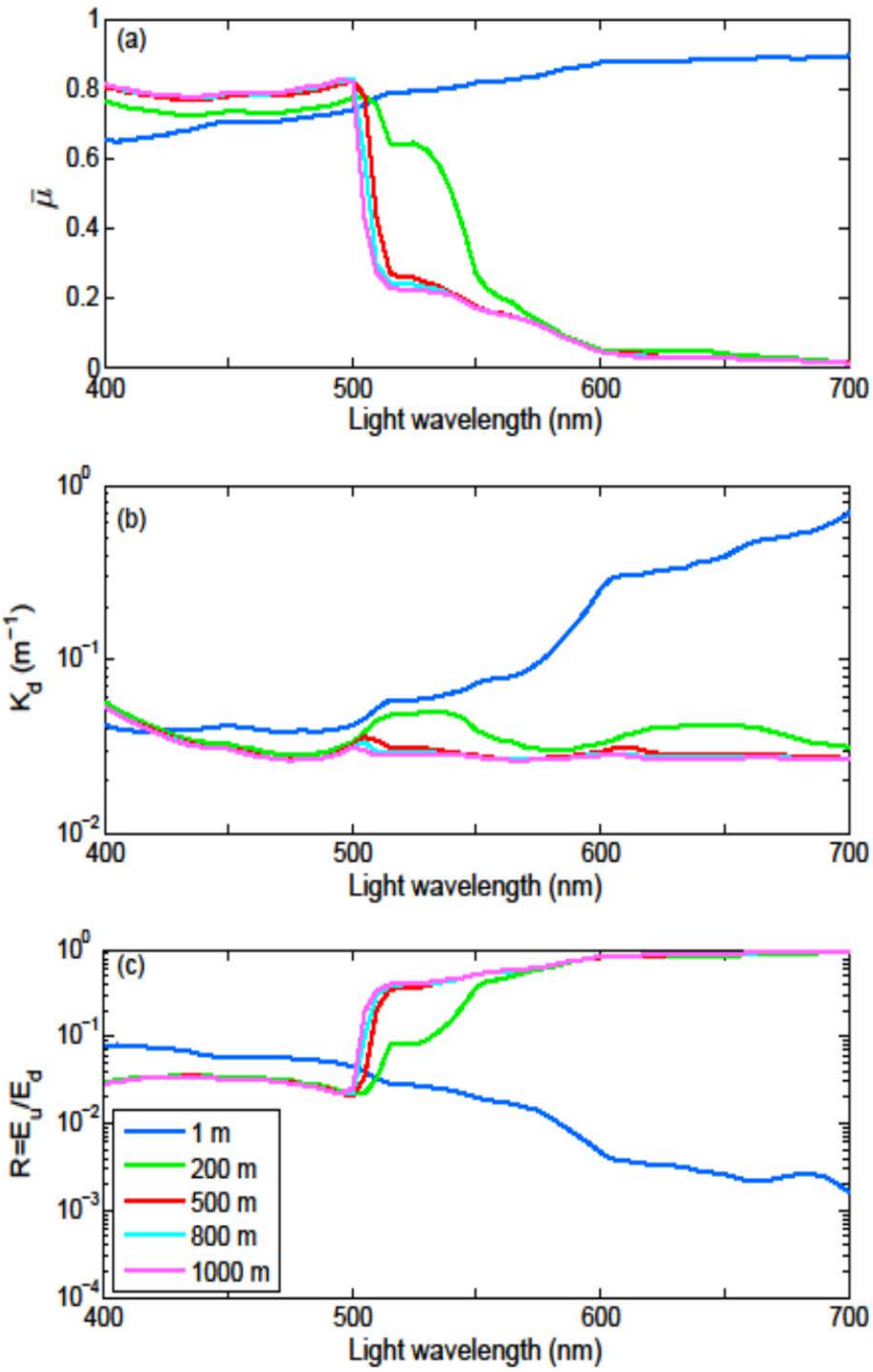

Figure 14: Spectra of apparent optical properties of the ocean at selected depths as indicated. (a) Average cosine of the total light field; (b) Diffuse attenuation coefficient for the downward plane irradiance; and (c) Irradiance reflectance. These results were obtained from simulations for clear sky conditions, solar zenith angle of 30°, and the chlorophyll-a concentration in the surface layer Chl = 0.2 mg m^{-3}. The inelastic radiative processes were included in the simulations.

As part of a previous report we showed examples of measurements of average light intensity at the six different directions accessible by the Omnicam instrument. It was apparent that the maximum depth for light detection with the current Omnicam hardware configuration is approximately 250 m. However, the system was inadequate for lower light observation with adequate signal to noise. As such, a new instrument to record deep sea light levels was designed, fabricated, tested, and the results published (Haag et al., 2014) A key design choice was the selection of the detector as a thermoelectrically-cooled multi-pixel photon counter (MPPC) module from Hamamatsu Photonics (Hamamatsu, SZK, Japan). The MPPC is essentially an SPM in that it consists of an array of avalanche photodiodes (APDs) operating in Geiger mode, resulting in high gain. Although the MPPC is a two-dimensional array, the signals from individual APDs are summed to provide a single value corresponding to the photon flux incident on the detector active area. To maximize light input to the system, a high-efficiency Lambertian (HiLAM) diffuser from RPC Photonics (Rochester, NY) was selected.

Two low-light radiometers were developed, each with a different spectral filter. Optical and detector system components are shown in Figure 15. The basic measurement process is as follows. External light incident on the optical port P is transmitted and illuminates the diffuser D. Light is then transmitted by the diffuser D and emitted with a Lambertian profile. The first lens L1 is located at a distance near its focal length from the diffuser D. Light transmitted by the diffuser D is then collimated by lens L1. The collimated light is reduced and transmitted by the filter S, and arrives at the second lens L2. The remaining light is then focused by lens L2 onto the active area of detector module M. The signal received by detector M is recorded to disk by the control computer. The tilt sensor/digital compass simultaneously records instrument position and orientation. Each radiometer system is enclosed in a cylindrical aluminum housing, pressure tested to 1000 m depth, with length 22.5” (57.15 cm) and diameter 4.5” (11.43 cm). The instrument housings were custom designed and machined from 6061-T6 aluminum alloy with Type III hard anodizing. External interfaces to the instruments were provided by wet-pluggable bulkhead connectors (SubConn, Pembroke, MA). Power is provided to each unit by a custom battery housing containing rechargeable lithium-ion battery packs. The instruments are controlled autonomously by small computers contained in the housings, which acquire and store data from the attached devices.

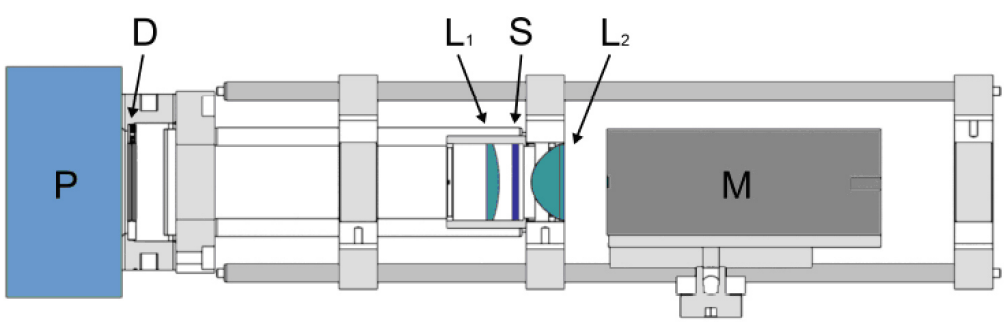

Figure 15: Schematic showing system components, including acrylic optical port (window) P, engineered diffuser D, lenses L_1 and L_2, spectral filter S, and detector module M.

The entire package in deployment is shown in figure 16. Sub image (a) shows a photograph of the system while (b) illustrates a block diagram of the components, as seen from the outside.

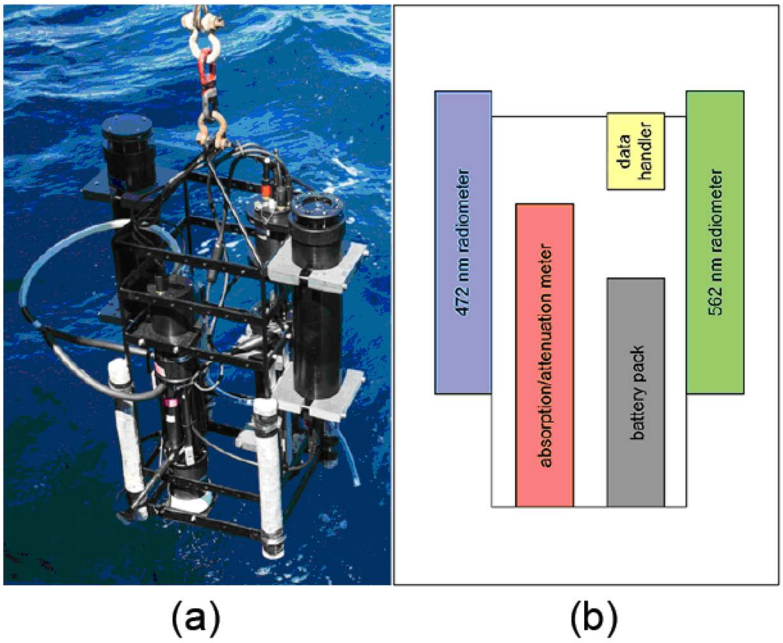

Figure 16: Mesopelagic light meter (MLM) field deployment package, including two low-light radiometers, absorption/attenuation meter with data handler, and rechargeable battery pack. (a) Actual photograph. (b) Component diagram.

Data was collected on two research cruises. The first cruise utilized the R/V New Horizon, managed by Scripps Institution of Oceanography (SIO), with held stations of the coast of San Diego, California, from April 1 to April 2, 2014. The second cruise utilized the R/V Atlantic Explorer, managed by Bermuda Institute of Ocean Sciences (BIOS), with held stations along a track from Barbados to Bermuda, from May 31 to June 8, 2014. An examples of data output is shown in Figure 17. Subimage (a) shows plots of recorded downwelling irradiance versus depth at the two measured wavelengths of 472 and 562 nm. A diffuse attenuation coefficient, derived from this data is displayed in (b).

As part of the research, data from the Atlantic Cruise (ABB) was compared to that obtained from the pacific one (PSD). A primary difference between the PSD and ABB profiles was the maximum available measurement depth. Downward irradiance $\mathbf{E}_d$ **(z; λ)** was acquired to depths of greater than 400 m during the ABB cruise, but was limited to approximately 300 m for the PSD cruise. Based on the collected attenuation coefficient **c (z; λ)** profiles, this was most likely due to the depth locations of layers of increased absorption and scattering. In the PSD cases, the peak attenuation region was generally found to be shallower than 50 m, whereas for the ABB cases, it was observed closer to, and occasionally exceeding, 100 m. The measurement depth ranges (differences between maximum and minimum depth) for ABB profiles were also nearly twice those for the PSD profiles. This indicates a more slowly changing light field for ABB profiles, since the available depth range is directly related to the dynamic range of the low-light radiometers. This was expected, since the **c (z; λ)** magnitudes were much higher for PSD profiles. Note that the maximum axis limits for **c (z; V)** plots are 0.4 m^{-1} and 0.2 m-1for PSD and ABB profiles respectively.

The diffuse attenuation functions for spectral downward plane irradiance $\mathbf{K}_d$ (**z;** 472) and $\mathbf{K}_d$ (**z;** 562) were also calculated, since these functions have been shown to not vary greatly with changing environmental conditions. Exploring the relationship between $\mathbf{K}_d$ (**z;** 472) and $\mathbf{K}_d$ (**z;** 562), particularly in the context of Raman scattering, was a key component of the present study. If the effects of Raman scattering are observed, $\mathbf{K}_d$ (**z;** 562) is expected to decrease with depth, relative to $\mathbf{K}_d$ (**z;** 472), until reaching an asymptotic value $\mathbf{K}_1$. Such a trend is observed in most of the ABB measurements, and is particularly clear in the ABB-S3-02 down-cast profile, where a nearly-asymptotic value appears to have been reached by approximately 280 m depth. For all ABB profiles, $\mathbf{K}_d$ (**z;** 562) was observed to be less than the pure water absorption coefficient at the green wavelength $\mathbf{a}_w$ (562), throughout the measured depth ranges, providing additional confirmation that Raman scattering acts to increase the magnitude of green wavelength light present in the water column. For the PSD profiles, it is likely that $\mathbf{K}_1$ was attained at depths shallower than those measured, as there was little relative change between $\mathbf{K}_d$ (**z;** 472) and $\mathbf{K}_d$ (**z;** 562) over the available depth range.

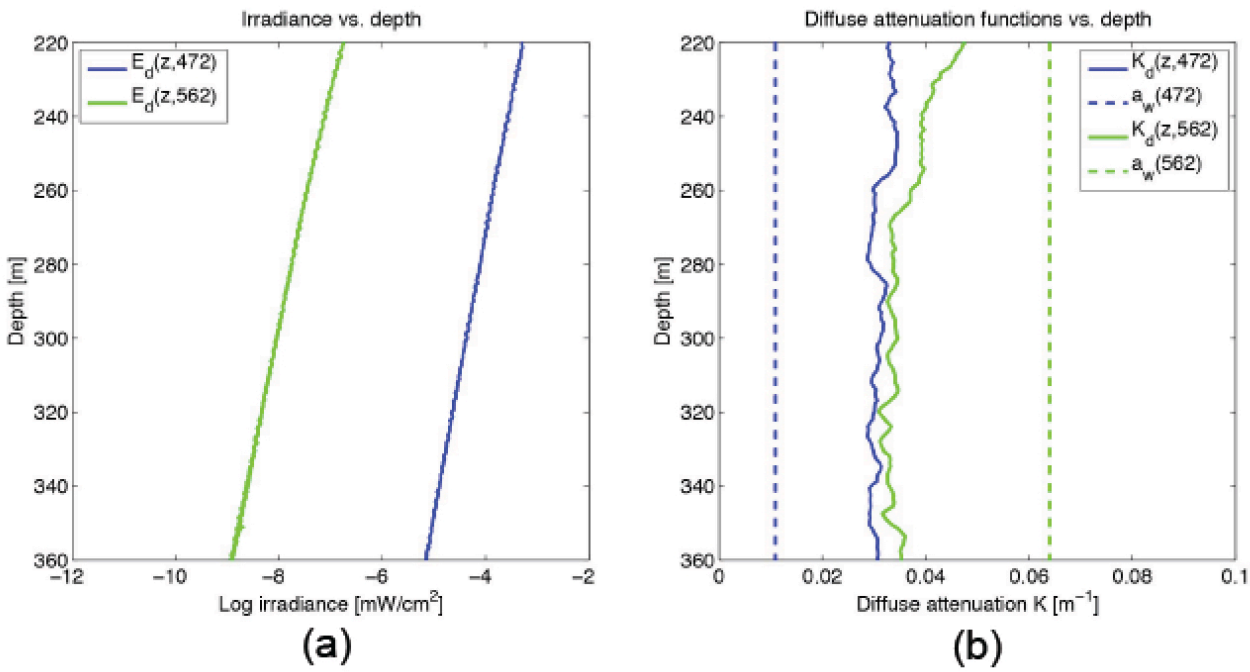

Figure 17: (a) Examples of measurement of downwelling irradiance in the blue (472 nm) and green (562 nm) as a function of depth. (b) Illustration of the relationship between diffuse attenuation $K_d(z,\lambda)$ and pure water absorption, $a_w(\lambda)$, for the green and blue channels.

BRDF measurements: A paper on the optical scatterometer for measurement of angular reflectance (OSMAR) instrument was published (Haag et al., 2013). The results presented therein correspond to a limited selection of the bidirectional reflectance distribution function (BRDF) data set collected from the 2012 *R/V Kilo Moana* research cruise off the Hawaiian Islands. Full processing algorithms were completed for the BRDF data in early 2013. For proper analysis of the data, geometric distortion correction, multiple exposure integration, and normal estimation are key aspects that must be considered. An example result from the full processing algorithm, including multiple exposure integration, is shown in Figure 18. Note that there is more intensity information in each processed BRDF map than can generally be displayed on a standard computer screen.

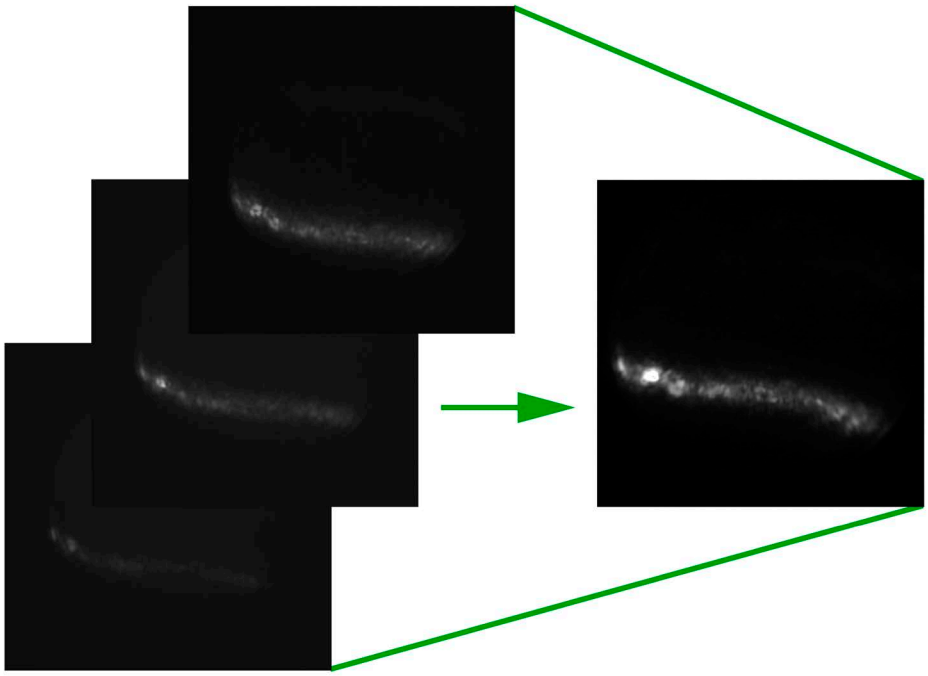

Figure 18: Example result from full BRDF data processing algorithm.

Objectives 2 and 3, visual physiology and camouflage behavior: Trials presenting *L. brevis* change color to *Palaemonetes* (shrimp) reveal that shrimp are unlikely to use visual stimuli as a cue to assess predator attack. Instead, we suspect they use a tactile assessment of water flow, but this demands further study. *P. latipinna* do respond to visual attack cues, and this work is ongoing. Our studies on *M. pfefferi* attack on mysids showed that these predators exhibit minimal variation in attack color change, consistently producing a stereotyped color change with most attacks. Thus we have been unable to assess the effectiveness of this attack behavior. However, we continue to assess this video footage for descriptive purposes.

Our review of proportion-based perception in animals points to a few predictions about the evolution of camouflage behavior. Specifically, we predict that for animals to achieve camouflage most efficiently, any error in matching a stimulus of a particular magnitude from the environment should fall on the side of higher magnitude in the range of stimulus variation. This is because due to proportional processing, potential predators cannot make as fine discriminations when assessing higher magnitudes as they can when assessing lower magnitude stimuli. Thus, animals that differ from a background by a small amount will be harder to detect if they are brighter than the background rather than less bright, for example.

Our investigations of *L. brevis* signaling suggest that these squid use mate signals in a unique way. Female signals are directed at males and indicate receptivity to mating. However, they do not elicit or repel male approach, and the multiple visual chromatophore components produced by females are used redundantly. We have preliminary data recommending an investigation of whether females have evolved more elaborate signaling in order to maintain visual contact with males during a mobile courtship that would be difficult in a turbid marine environment.

The Jaffe Lab coordinated closely with that of Johnsen in order to analyze results of experiments that were accomplished with the Squid Holodeck. Breifly, Cuttlefish are cephalopods capable of rapid camouflage responses to visual stimuli. However, it is not always clear to what these animals are responding. Previous studies have found cuttlefish to be more responsive to lateral stimuli rather than substrate. However, in previous works, the cuttlefish were allowed to settle next to the lateral stimuli. In this study, we examine whether juvenile cuttlefish (*Sepia officinalis*) respond more strongly to visual stimuli seen on the sides versus the bottom of an experimental aquarium when the animals are not allowed to be adjacent to the tank walls. We used the Sub Sea Holodeck, a novel aquarium that employs plasma display screens to create a variety of artificial visual environments without disturbing the animals. Once the cuttlefish were acclimated, we compared the variability of camouflage patterns that were elicited from displaying various stimuli on the bottom versus the sides of the Holodeck. To characterize the camouflage patterns, we classified them in terms of uniform, disruptive, and mottled patterning. The elicited camouflage patterns from different bottom stimuli were more variable than those elicited by different side stimuli, suggesting that *S. officinalis* responds more strongly to the patterns displayed on the bottom than the sides of the tank. We argue that the cuttlefish pay more attention to the bottom of the Holodeck because it is closer and thus more relevant for camouflage.

After each cuttlefish response was classified into one of the twelve camouflage categories, all the responses were divided into five groups based on the five bottom stimulus patterns. Within each group, we calculated the proportion of cuttlefish responses in each of the twelve categories. For example, out of all the cuttlefish responses to the television static bottom, we calculated the proportion of those responses in the 50% mottled, 50% disruptive camouflage category. We followed this same methodology for the side stimulus patterns. That is, using all of the cuttlefish responses we calculated the proportion of responses in each of the twelve camouflage categories for each of the five side stimulus groups. Comparisons of the proportion of responses in each of the camouflage categories were then made within and across each of the groups.

To more easily compare responses to stimulus patterns, we calculated the center of mass for the responses to each of the bottom and side stimuli as shown in Figure 19 (below). That is, using the proportion of responses in each of the twelve categories for each stimulus, we calculated the average response. To quantify the error, we calculated 95% bootstrap confidence intervals. That is, out of all the responses to a given bottom or side stimulus, we resampled with replacement from those responses to obtain a subsample of the same size as the original sample. We repeated this process 10,000 times to obtain 10,000 subsamples of the responses to each of the bottom stimuli and each of the side stimuli. We then calculated the average response for each of those subsamples, and the 95% of average responses that were closest to the original sample mean were used to delineate the bootstrapped confidence intervals shown in Fig. 7. Due to the nature of the data (compositional with structural zeros), we used a separate Kruskal-Wallis test for the percent mottled, disruptive, and uniform in camouflage responses to test if there were significant differences among bottom stimuli groups and side stimuli groups. When appropriate, we used a post-hoc test with a Dunn-Sidak correction to investigate which groups were significantly different.

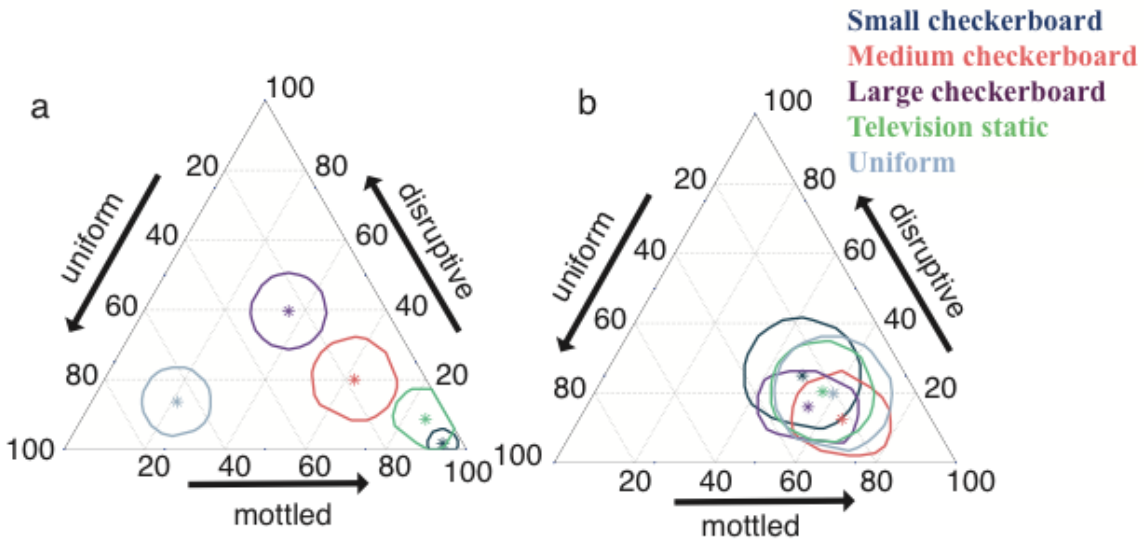

Figure 19: Average response of cuttlefish to each of the five stimulus patterns. The asterisk indicates the average value, and the surrounding shapes are the bootstrapped 95% confidence intervals. (a) Average response to different bottom stimuli. (b) Average response to different side stimuli.

The elicited camouflage patterns from different bottom stimuli were more variable than those elicited by different side stimuli, suggesting that *S. officinalis* responds more strongly to the patterns displayed on the bottom than the sides of the tank. We argue that the cuttlefish pay more attention to the bottom of the Holodeck because it is closer and thus more relevant for camouflage.

Additional work on image classification: Although not initially envisioned as part of this program, as the Jaffe Lab became more and more involved with the analysis of the cuttlefish patterns it became obvious that automated techniques for classification would be of great value. As such, students were recruited to undertake these efforts and they have been largely successful. In a recent submission by Orenstein et al. (Orenstein, 2015) automated the processing of cuttlefish camouflaging behavior that captured ~12,000 images of the animals' response to changing visual environments. The computer vision work presented an automated segmentation and classification workflow to alleviate the human processing this complex data set. Breifly, the specimens' bodies are segmented from the background using a combination of intensity thresholding and Histogram of Oriented Gradients. Subregions are then used to train a texton-based classifier designed to codify traditional, manual methods of cuttlefish image analysis. The segmentation procedure properly selected the subregion from ~95% of the images.. The classifier achieved an accuracy of ~94% as compared to manual annotation. Together, the process correctly processed ~90% of the images. Additionally, we leverage the output of the classifier to propose a model of camouflage displays that attributes a given display to a superposition of the user defined classes.

Polyphenism in Sepia: We investigated how the body patterns used by the cuttlefish *Sepia officinalis* change over time and with repeated exposure to a range of backgrounds. The detection of camouflaged prey by predators in visually complex environments is no trivial task. One way in which predators can reduce search time and effort is via a search image, by which the visual system picks out shapes or other features that fit a mental "template" drawn from previous experience of the same prey type. This acts to alleviate the need for detailed attentive searches of an entire scene. Animals using adaptive

camouflage might be less susceptible to detection via search image if they can alter characteristics of their body patterns without compromising on the overall effectiveness of their camouflage. This idea is somewhat in contradiction to the current understanding that the body pattern responses are rather "hard-wired" responses resulting from specific visual cues in the background. Experiments using *S. officinalis* usually assume body patterns are stable after a certain period of acclimation to a new visual environment. We carried out a series of experiments to test how stable characteristics of cuttlefish body patterns were in response to a range of backgrounds containing varying degrees of visual complexity (Figure 20). We have applied novel image processing techniques (figure 21) to determine the variability and the areas of change in individual animal responses a) over an hour period on each background; b) over five consecutive days; c) on backgrounds of differing visual complexity, as well as between animals. We are currently in the process of analyzing data from these experiments.

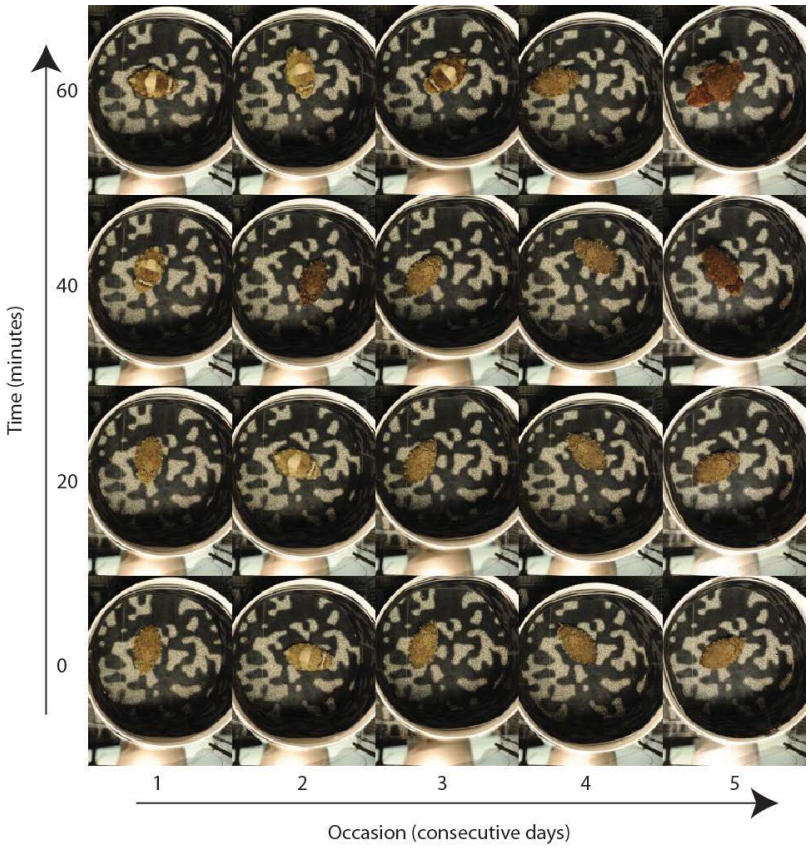

Figure 20: Responses of a single cuttlefish (*Sepia officinalis*) to one of the x backgrounds tested, showing that body patterns are often prone to vary over both the hour test period (following acclimation) and with repeated exposure over a 5 day period.

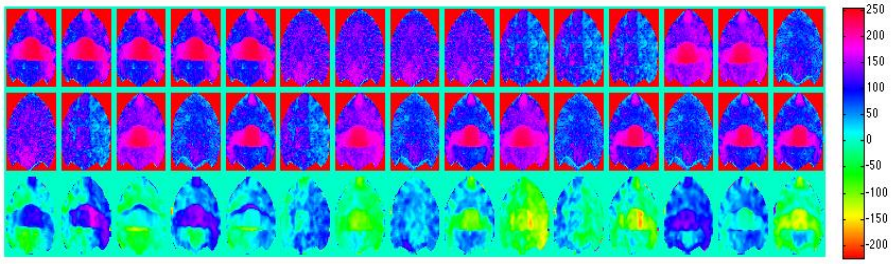

Figure 21: Illustrating image processing to identify regions and extent of variability, here of the individual animal and background shown in figure x at all times on occasion 1. Interestingly, it highlights asymmetry in body patterns.

In shipboard behavioral experiments, we found evidence for rapid switching between transparency (under ambient light) and red pigmentation (with the addition of a directed beam of light) in juveniles of two species of mesopelagic cephalopod, the bolitaenid octopus *Japetella heathi* and the onycoteuthid squid *Onychoteuthis banksii*, which are found at depths where both strategies would be useful (Figure 22). These rapid (<1 second in *O. banksii*) changes are achieved via the expansion and contraction of chromatophores. Our findings are consistent with a strategy to optimize camouflage under both ambient and bioluminescent searchlight viewing conditions. We also show that the response is strongest to blue light, while it is absent under red light, consistent with the known sensitivities of most deep-sea taxa as well as the emission spectra of most searchlight photophores.

Figure 22: **Japetella heathi** ***in normal transparent state and after being illuminated with a directed beam of light.***

In collaboration with groups in Europe we also investigated two camouflage phenomena in the cuttlefish *Sepia officinalis*.

a) The ability to fill in missing visual information (contour completion, often achieved through modal or amodal completion) is important for animals utilizing camouflage: failure to recognize objects as whole when faced with ambiguous information (e.g. occlusions) could result in the animal responding with a body pattern unsuitable for the local visual environment. We found evidence, through a continuation of previous work into edge detection mechanisms, that cuttlefish are able to fill in missing visual information and perform contour completion as conferred by their body patterns (Figure 23).

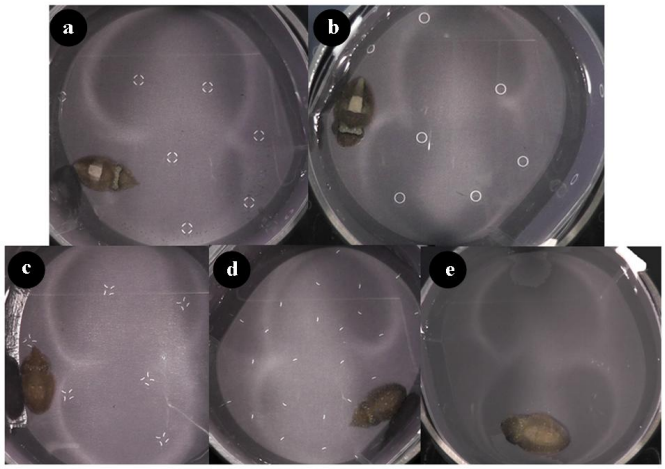

Figure 23: Completion of illusory contours: a) Fragmented contour information is completed when configured to still provide information as to the object, resulting in a body pattern indistinguishable from b; b) full circles (positive control); c) Rotated yet still clustered fragments of circles of the same size do not provide the necessary information for completion, causing each fragment to be interpreted as individual pieces as in d; d) scattered fragments of circles; e) uniform grey background (negative control).

b) Pictorial depth cues are used effortlessly in human vision to integrate aspects of three-dimensionality to our visual experience of the world. For example, shading gives information pertaining to the directionality of the dominant light in a scene, as well as information about the convexity/ concavity of objects. The power of such cues becomes obvious if we consider how easily we interpret depth cues from 2-D images such as photographs. The cuttlefish *S. officinalis* has been cited as using shading of the so-called "White Square" body pattern component to convey the impression of convexity to some body patterns in keeping with objects in the local environment. We investigated, through behavioral experiments, how light directionality and pictorial cues might interact in the strength and positioning of the White Square shading. Data will be analyzed to assess both the perceptual experience of the cuttlefish (and how this compares to that of humans), and how shading might enhance the effectiveness of camouflage by providing cues consistent with the local environment and hence preventing the animal from standing out to potential predators (Figure 24).

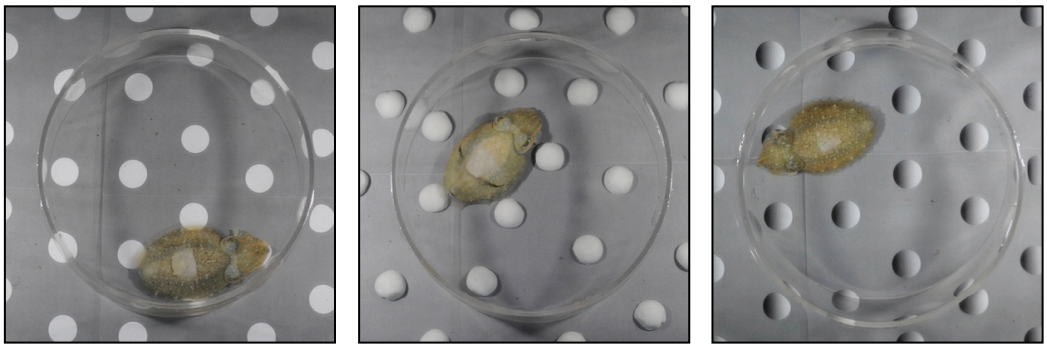

2-D objects | 3-D objects | 2-D objects + pictorial depth cues

Figure 24: Subset of test stimuli used to investigate the interaction of lighting and pictorial depth cues. Here all stimuli are lit equally from both sides; further tests restricted light directionality to one side.

Point Spread Function of fish lenses: Cephalopods are viewed by a variety of visual systems, each trying to break their camouflage, detect, and recognize them. This visual process starts with the optics of the potential viewer, where the lens modulates the image of the camouflaging cephalopod and its surroundings before the retina registers the image. While the modulation of the signal can deteriorate some of the spatial features in the scene other details are made clearer, which may play a part in camouflage breaking. The point spread function (PSF) of an animal lens can be measured by quantifying how much, and in what way, a point source of light spreads through it (figure 25). A PSF can then be used to characterize the optics of the animal, and even model the propagation of information through the animal's visual pathway. To better understand what spatial information is maintained by potential predators seeking to break cephalopod camouflage, the PSF of lenses from 24 mesopelagic and bathypelagic animals were obtained and analyzed. Results suggest that the optics of each species are well suited to their environment and predation.

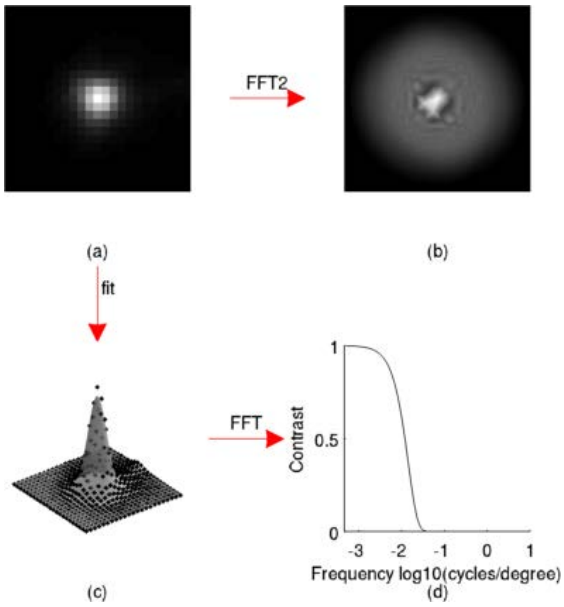

Figure 25: Point Spread Function (PSF) analysis. (a) The actual PSF was measured using specially built apparatus. (b) The Fourier Transform of the PSF resulted in a 3 dimensional Modulation Transfer Function (MTF) of each lens. (c) A Gaussian function was fit to the data and used to calculate a 2 dimensional MTF for statistical comparisons between the viewing animal species.

Bioelectric crypsis: Sepia officinalis decreased motion and bioelectric stimuli in response to an approaching predator stimulus (Figure 26). The amplitude of body movements and voltage was decreased by 42% and 16%, respectively, at the onset of the stimulus. The frequency of body movements and the bioelectric field were reduced by 59% and 45%, respectively. Bonnethead and blacktip sharks responded to the jetting stimulus (200**µ**V) significantly more than the resting stimulus (30**µ**V) (Figure 27). Sharks responded to the freeze stimulus (10**µ**V) significantly less than jetting and resting stimuli ($P<0.0001$). Detection of electric stimulus is distance dependent and larger electric fields are detected at a greater distance. The freeze response decreased detection distance by 2.4cm relative to the resting stimulus, whereas the jetting stimulus increased detection distance by 14.2cm. These results suggest that cuttlefish may experience a decrease in predation risk by reducing motion and electric stimuli used by foraging shark predators.

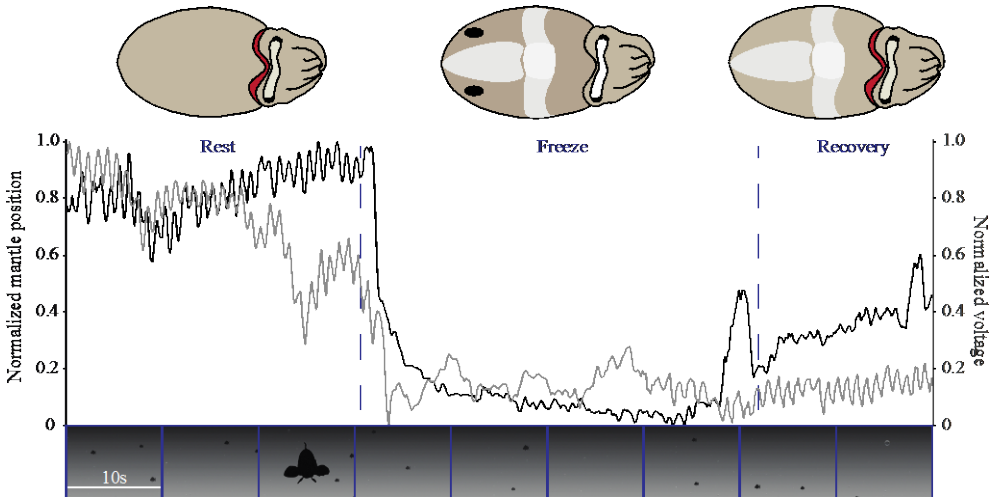

Figure 26: Representative response of* Sepia officinalis *to a video simulation of a looming predator. Both the frequency and amplitude of body movements and bioelectric cues were reduced by the freeze response. Amplitude data are normalized to the peak point in each trace for presentation purposes. Cuttlefish illustrations depict the typical camouflage and mantle cavity opening states for each phase of the recording. Rest = quiescent, non-active animals. The gills were exposed laterally at the mantle cavity opening at the junction between the mantle and the head. Freeze = response characterized by motionlessness, flattening of the body, covering of the gills, and reductions in the amplitude and frequency of electrical cues. Recovery = transition from freeze response to the resting state. Camouflage and the amplitude and frequency of body movements and electric potential returned to within 1 standard deviation (s.d.) of the resting state at the beginning of the recovery period. Resting mantle height and baseline voltage returned to within 1 s.d. of resting at the end of the recovery period (not shown). Black/primary y-axis= body movement/motion, grey/secondary y-axis= electric potential/voltage.

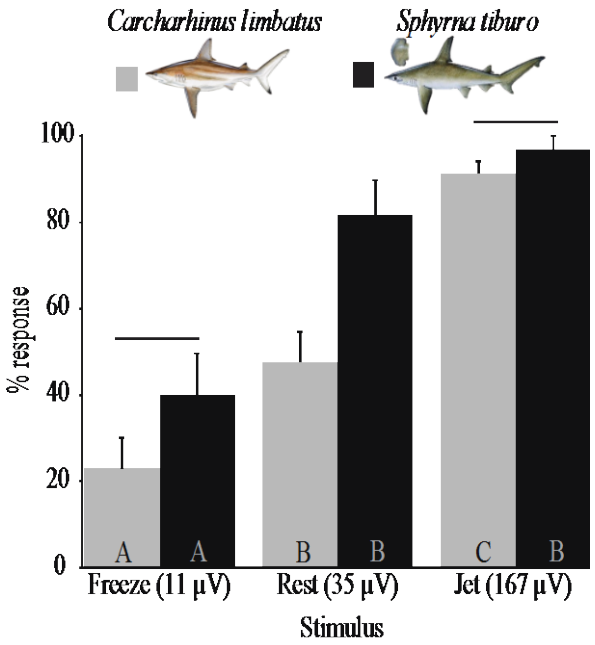

Figure 27 : Shark detection of Sepia- simulating electric fields. Bonnethead sharks responded to freeze and jet-simulating electric stimuli significantly more frequently than blacktip sharks. Both species demonstrated the greatest proportion of responses to jet-simulating stimuli, with nearly 100% of encounters resulting in a bite response. Both species also demonstrated the fewest responses to the freeze-simulating stimuli. Bars represent the mean percent responsiveness ± standard error (s.e.). The lines connecting bars indicate no difference between species (α= 0.01). Bars for each species that share the same letter were not significantly different (α= 0.01).

Cuttlefish toxicology: Both species of cuttlefish possessed tetrodotoxin-containing tissues (TTX^+) that ranged from 0.02ng/mg of tissue to 2.2ng/mg of tissue measured by the immunoassay. In contrast, the blue-ringed octopus, one of the most venomous and lethal cephalopods, exceeds TTX concentrations of 100µg/g in some tissues. Though our analyses did yield TTX^+ tissues, they suggest that TTX is not used for delivering lethal bites as in the blue-ringed octopus. Blue-ringed octopuses have the highest concentration of TTX in the posterior salivary glands, which are associated with the feeding apparatus and are used to paralyze prey before consumption and deter predators from attack. Blue-ringed octopuses also deliver high concentrations of TTX to their eggs in order to protect developing embryos from predation events. The gonads (including eggs) and salivary glands were among the most common TTX^+ cuttlefish tissues, although TTX was also identified in the skin, ink, and digestive organs of some individuals for both species. The greatest concentrations of TTX in both species were found in the gonads, salivary glands, and cardiorespiratory structures. Concentrations in these tissues were 4-6 fold greater than the digestive structures, skin and ink. Although the concentrations of TTX were not significantly different between species, *Metasepia* typically yielded concentrations that were nearly double those of the same tissue of *Sepia* (Figure 28). However, because the total amount of TTX in individual cuttlefish was far below the lethal limit seen in blue-ringed octopuses and the concentrations of TTX were not different between cuttlefish species, the conspicuous coloration of *Metasepia* is not likely used as a warning of toxicity. Preliminary behavioral work on prey consumption of *Metasepia* and *Sepia* individuals further supports this hypothesis; predators readily consumed, and therefore, were not deterred by, the TTX in either species.

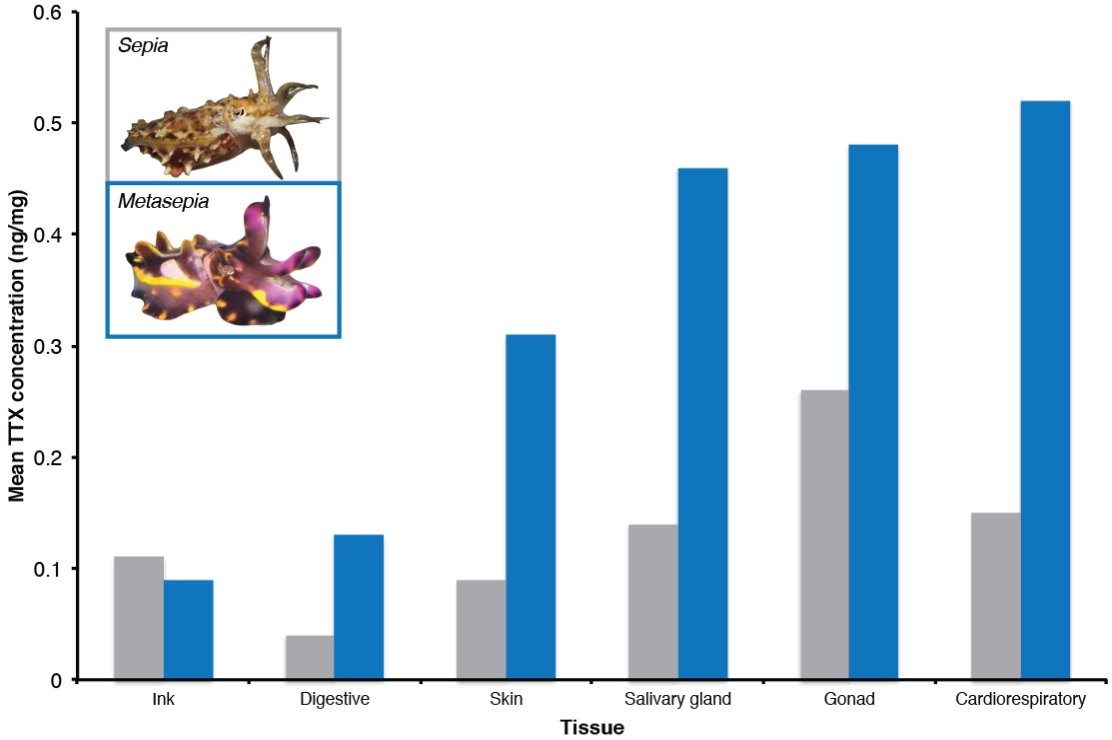

Figure 28:* Metasepia *tissues had nearly double the TTX concentration of* Sepia *tissues. The highest concentration of TTX for both species were found in the salivary glands, gonads, and cardiorespiratory system. The salivary glands and gonads also demonstrate the greatest levels of TTX in tissues collected from lethal blue-ringed octopuses. TTX concentrations (in ng/mg of tissue) were quantified using a competitive inhibition enzyme immunoassay (CIEIA).

Cuttlefish feeding kinematics: Using high-speed videography, we quantified kinematic variables of tentacular feeding strikes in two cuttlefish species of similar size, but which exhibit differences in morphometrics of the feeding tentacles (Figure 29). Flamboyant cuttlefish, *Metasepia pfefferi*, extended their long and slim tentacles approximately 2.2 body lengths, whereas dwarf cuttlefish, *Sepia bandensis*, extended their shorter and wider tentacles an average of 1.7 body lengths (Figure 30). *Metasepia* completed the rapid strike in less than 10ms, two times faster than *Sepia*. Although most species of ballistic foragers share similarities in the phases of strike behavior (attention, positioning, and strike), cuttlefish tentacle extension exceeded that measured for all other species thus far. The longest reported extension of a ballistic feeding appendage occurs in *Chameleo* species, with a maximum extension of approximately 1.5 body lengths (Figure 30). *Metasepia* strike duration was similar to that of the fastest strikes of plethodontid salamanders, while *Sepia* strike duration was slightly slower and more similar to those of *Chameleo*. Our results suggest that the physical properties of water do not constrain performance of feeding strikes in these aquatic ballistic-style foragers and that differences in kinematics are likely due to morphological structures.

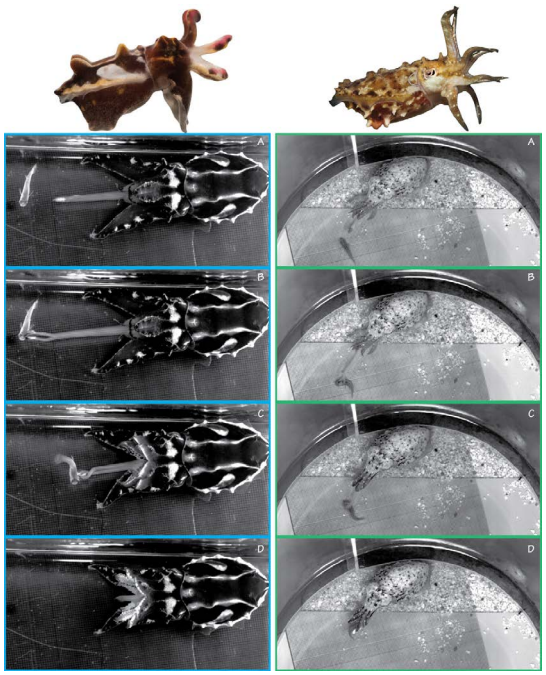

Figure 29: High-speed video feeding sequences recorded at 3000fps from* Metasepia pfefferi *(left column; blue) and Sepia bandensis (right column; green). A. Slow-phase tentacle extension and alignment. B. Fast-phase extension and capture. C. Fast-phase recoil and torsion. D. Consumption.

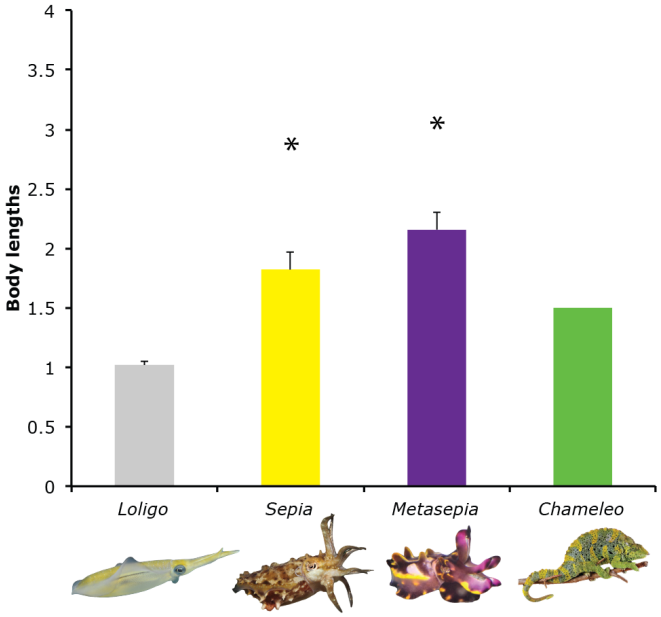

Figure 30: Mean feeding appendage extension (standardized to body length) for* Loligo *squid tentacles (Kier and van Leeuwen 1997),* Sepia *cuttlefish tentacles (present study),* Metasepia *cuttlefish tentacles (present study), and* Chameleo chameleon *tongues (de Groot and van Leeuwen 2004). Cuttlefish extended their feeding tentacles a greater distance than other taxonomic groups that use a protusible feeding appendage for prey capture. Maximum extension by a single individual is indicated by a *.

Camouflage breaking using polarization vision: Because light in the pelagic environment is partially polarized, it has been suggested that the polarization sensitivity found in certain pelagic species may serve to enhance the contrast of their transparent prey. We examined the potential for this during cruises in the Gulf of Mexico and Atlantic Ocean and at a field station on the Great Barrier Reef. First, we collected various species of transparent species and micronekton and photographed them between crossed polarizers. Many groups, particularly the cephalopods, pelagic snails, salps and ctenophores, were found to have ciliary, muscular or connective tissues with striking birefringence. *In situ* polarization imagery of the same species showed that, while the degree of underwater polarization was fairly high (~30% in horizontal lines of sight), tissue birefringence played little to no role in increasing visibility. This is most likely due to the low radiance of the horizontal background light compared to the downwelling irradiance. In fact, the dominant radiance and polarization contrasts of the object are due to unpolarized downwelling light that has been scattered from the animal viewed against the darker and polarized horizontal background light. We also showed that relatively simple algorithms can use this negative polarization contrast to substantially increase visibility.

Another long-held hypothesis is that polarization vision in the water column is used to break the mirror camouflage of silvery fish, since biological mirrors can change the polarization of reflected light. While the addition of polarization information likely increases the conspicuousness of silvery fish at close range, direct *in situ* evidence that silvery fish, or indeed any pelagic animals, are visible at longer distances using polarization vision than they are when using radiance vision is lacking. We combined *in situ* polarization imagery with novel models of visual detection that allowed us to directly compare the sighting distances of underwater animals when viewed by polarization-sensitive and polarization-insensitive visual systems. We found that, in general, the sighting distances of the lateral surfaces of these animals was shorter for polarization vision than for radiance vision. The primary factors limiting the polarization sighting distances are the relatively low degrees of polarization of underwater light and the low polarization sensitivity of the microvilli in photoreceptors. The lateral surfaces of silvery fish may be particularly hard to detect via polarization vision in horizontal viewing because the incident light that is reflected is generally similar to the background in both radiance and polarization.

Objective 4, biophotonics: Skin cells of octopi, squids and cuttlefish exhibit a remarkable ability to rapidly change color and reflectivity for camouflage and communication. Neurotransmitter signaling to the skin triggers synergistic changes in the refractive index, thickness and spacing of subcellular Bragg reflectors, producing dramatic changes in both the wavelength and intensity of iridescence. We discovered that iridescence (angle-dependent colored reflectance) is controlled by a neurotransmitter-activated signal transduction cascade culminating in catalytic changes in phosphorylation of unique "reflectin" proteins, the major constituents of the membrane-bound Bragg lamellae. Acting as a molecular switch controlled with hair-trigger sensitivity, the resulting neutralization of the cationic reflectins overcomes their Coulombic repulsion, allowing their reversible, 2-step condensation and subsequent hierarchical assembly. In vitro analyses with the purified recombinant reflectins and molecular modeling suggest that the first stage of conformational condensation drives the emergence of secondary folding of the canonical repeat units in these proteins to form amphiphilic alpha-helices, and that these newly emergent structures present bifacially phase-segregated hydrophobic faces that can act as molecular Velcro-like patches that mediate further tertiary and quaternary condensation and hierarchical assembly. This assembly masks surface charges on the reflectins, thereby triggering a compensatory efflux of small ions across the lamellar membranes that subsequently drives a Gibbs-Donnan-mediated expulsion of water, shrinking the thickness and spacing of the Bragg lamellae while increasing their refractive index. The result is a progressive change of color of the reflected light across the visible spectrum, with a sharp increase in the intensity of reflectance. The process is reversible and

finely tunable, allowing selective reflection of any color. This system we discovered is one of the most subtle protein-mediated signal transduction systems yet discovered, and the first to be found that regulates a tunable biophotonic function without any chromophores - determining the formation of reconfigurable nanostructures that change their interaction with light. Translation of the underlying mechanisms may open new approaches to dynamically reconfigurable, nanostructured materials and tunable photonic systems.

The range of colors reflected by the activated skin cells, and details of the nanoscale Bragg lamellae responsible for this tunable reflectance, are shown in Figure 31:

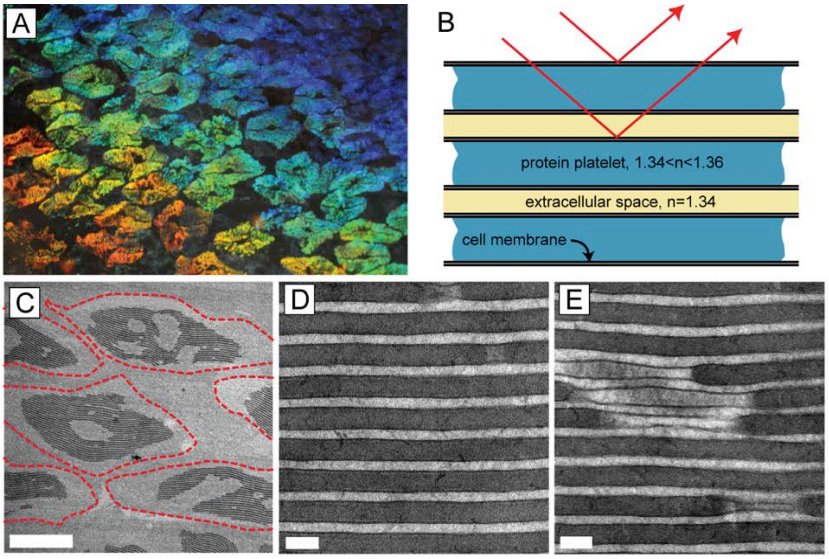

Figure 31: Intracellular structure of dermal iridocyte in the squid, Doryteuthis pealeii. (A) Darkfield image of* Doryteuthis pealeii *skin (40X magnification) under white light. Iridocyte cells appear flat in the plane of the tissue; avg. size ca. 20-40 μm wide x 2-5 μm thick. Application of the neurotransmitter ACh at upper right induced activation of a wave of colored reflectance. The dark area in the center of each cell corresponds to the position of the cell nucleus. (B) Schematic showing the components of the intracellular Bragg reflector. (C-E) TEM images of ultrathin cross-sections of green iridocyte cells fixed with uranyl acetate: (C) scale bar = 5 μm; (D) scale bar = 200 nm; (E) scale bar = 200 nm. Dark, electron-dense areas correspond to protein-filled lamellae; cell boundaries are outlined in red for clarification.

We elucidated the sequential, reversible molecular and electrostatic interactions operating over multiple length scales to drive the dynamic evolution of secondary, tertiary, and quaternary structure of proteins and the membrane structures that encapsulate them to yield rapidly and reversibly tunable color and brightness in the tunable iridocytes (Figure 32) and broad-band reflectivity in the closely related, switchable bright white leucophore cells in squid skin.

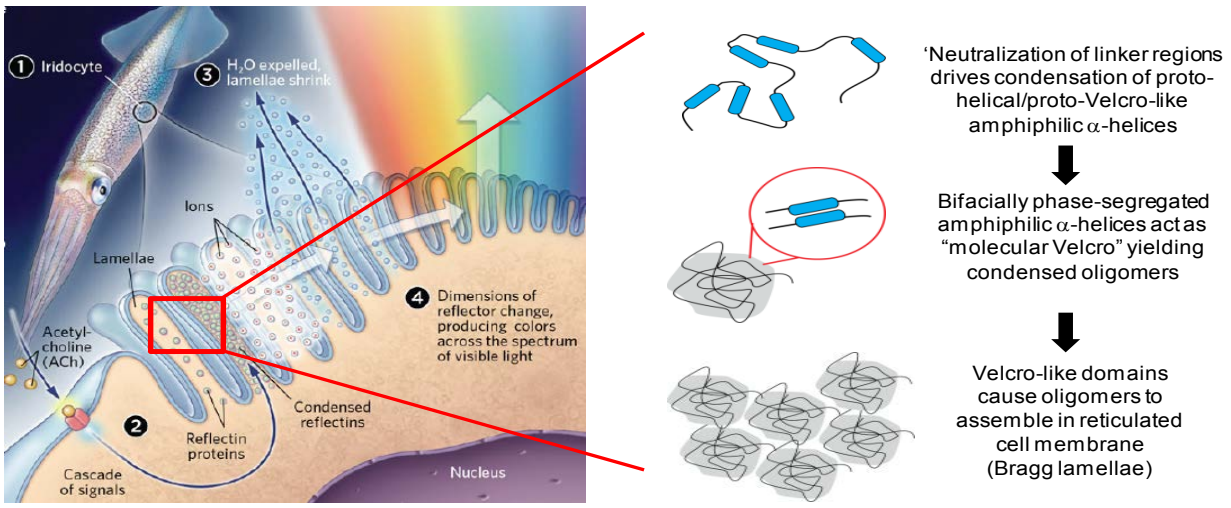

Figure 32: (Left:) Bragg lamellae in the squid iridocyte cell dynamically change spacing and refractive index contrast through influx/efflux of water due to Gibbs-Donnan equilibrium that is triggered by the neurotransmitter-induced, signal transduction-mediated phosphorylation and resulting charge-neutralization of the metastable reflectin proteins, as explained in detail below. (Right:) Charge neutralization of histidine side chains in the metastable reflectins leads to secondary structure development, creating bifacially phase-segregated amphiphilic α-helices that act as 'molecular Velcro', driving the further, hierarchical assembly of condensed oligomers. This tunably reversible control of reflectin condensation and assembly triggers the ionic flux that activates Gibbs-Donnan-mediated efflux of water [as monitored directly with D_2O tracer] that shrinks the Bragg lamellae to produce the tunable change in reflected wavelength

In these systems, we discovered, a neurotransmitter-activated signal transduction cascade culminates in activation of a specialized enzyme catalyst (a protein kinase) that phosphorylates specific sites on the "reflectin" proteins, thus neutralizing the charge on these cationic proteins, thereby overcoming their Coulombic repulsion and allowing their reversible condensation. This condensation, in turn, triggers a compensatory efflux of small ions across the membranes (either lamellar, in the color-producing iridocytes, or vesicular, in the switchable white leucophores), that in turn drives a Gibbs-Donnan-mediated efflux of water from the membrane-enclosed structures containing the proteins, simultaneously increasing the refractive index contrast and changing (in the case of the iridocytes) the thickness and spacing of the lamellae (cf. Figure 32). The result is a finely tunable and reversible change in the intensity and color of light reflected from the accordion-like folds of the membrane that we showed form the Bragg lamellae (Figure 33):

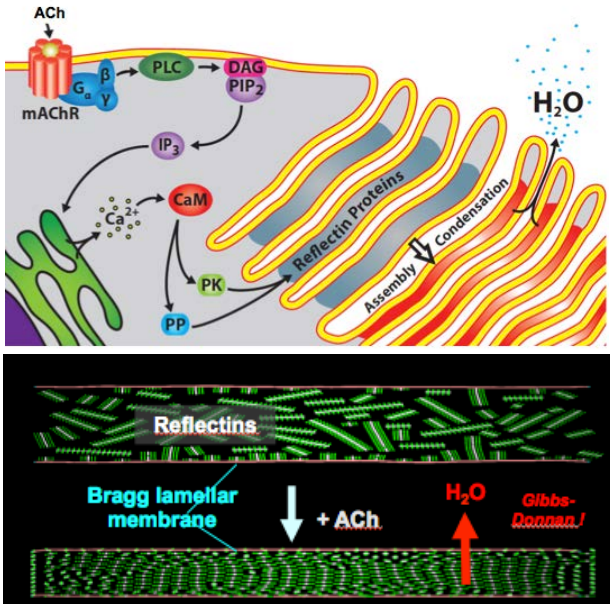

Figure 33: (Top:) Molecular details of the neurotransmitter (ACh)-triggered signal transduction cascade culminating in activation of the enzymatically catalyzed phosphorylation of reflectins, driving their condensation, with the resulting re-equilibration of electrostatic potential and osmotic pressure driving dehydration of the Bragg lamellae. (Bottom:) Diagram illustrating the Gibbs-Donnan-mediated reversible efflux of water, tuning the thickness and spacing of the Bragg lamellae, following condensation of the reflectin proteins that also increased the refractive index contrast (thereby activating reflectance).

The same mechanism operates in the switchably bright white leucophores, we found. But the different morphology of the reflectin-enclosing membranes in these cells (as discoidal vesicles rather than lamellae) yields slightly different photophysics, in which the Gibbs-Donnan dehydration of the vesicles produces white (broadband) Mie-scatterers (cf. Figure 34].

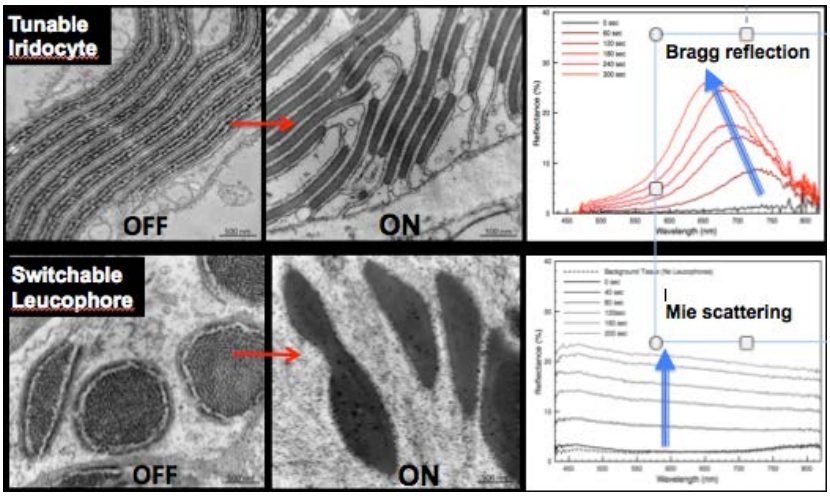

Figure 34: Tunably colored iridocytes (top row) vs. switchably bright white leucophores (bottom row). TEMs and spectral analyses show the different structures of the reflectin-containing membranes both before ("off") and after ("on") addition of the neurotransmitter, ACh, and the resulting differences in photophysical responses (right). The molecular mechanism is the same for both; the different architectures produce the different photonic behaviors.

In vitro analyses with the purified recombinant reflectin proteins confirmed that reversible assembly of the metastable reflectin proteins is the driver of this finely tuned transition, controlled with hair-trigger sensitivity by small changes in the enzymatically amplified, signal-transduction-mediated, phosphorylation/dephosphorylation of specific sites on the proteins that reversibly neutralize the positive charges of histidine residues. As this neutralization overcomes electrostatic repulsion of the initially cationic reflectins, the resulting condensation of the proteins drives the start of secondary folding of the canonical "repeat" units in the reflectins to form amphiphilic α-helices. These newly emergent amphiphilic helices uniquely present bifacially phase-segregated hydrophobic faces that act as molecular Velcro-like patches to drive further tertiary and quaternary condensation and hierarchical assembly (cf. Figures 35-37):

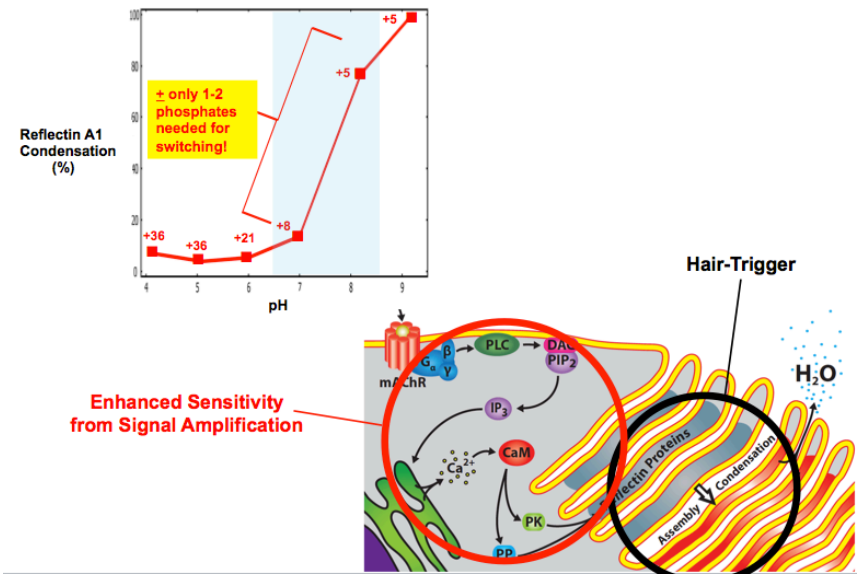

Figure 35: Condensation of the reflectins is driven by neutralization – resulting either from phosphorylation in vivo, or (as shown here), by titration of recombinant reflectin A1 with changes in pH as an in vitro surrogate for phosphorylation. Neutralization of the net positive charge of the histidine imidazole nitrogens overcomes Coulombic repulsion and drives condensation (monitored here spectrophotometrically). Pale blue indicates the range of physiological pH; numbers in red are the calculated net positive charges on reflectin A1; the steep sigmoidal curve in the physiological pH range indicates that metastability of the reflectin is poised with a hair trigger between the uncondensed and condensed states. Results for the other three reflectins found in the tunable Bragg lamellae are similar.

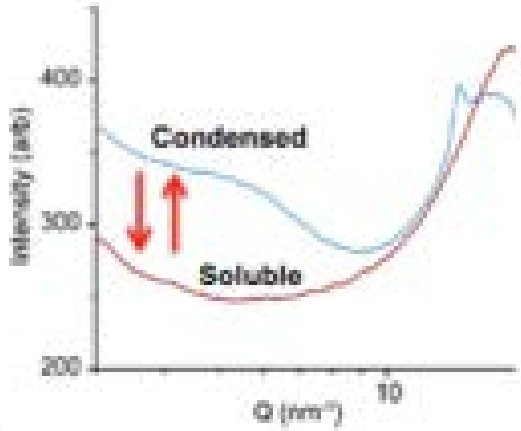

Figure 36: WAXS (wide-angle X-ray scattering) data show that the reflectins are initially "unstructured", but reversibly acquire secondary and higher-order structure as they are triggered by neutralization to condense.

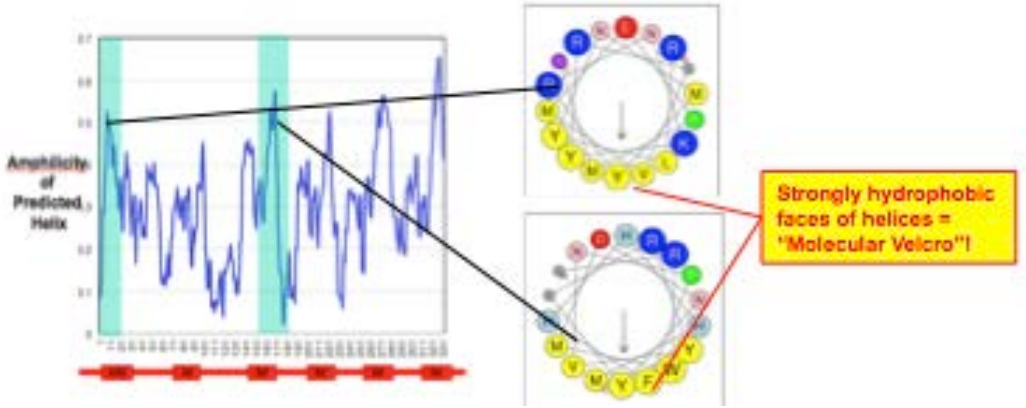

Figure 37:. Condensing reflectin "repeat" domains fold to form bifacially phase-segregated amphiphilic helices, each presenting a hydrophobic "molecular Velcro-like" surface. (Left:) Calculated amphiphilicity of predicted helical domains, mapped over the corresponding structure of reflectin A1 (in red, below), showing that highest amphiphilicity is predicted for regions corresponding to the canonical "repeat" domains in the molecule (shown as thicker red blocks. (Right:) Representations of two of the predicted α-helices, showing the hydrophobic amino acid sidechains in yellow; those negatively charged in red, and positively charged in blue. Analyses show similar patterns for the other 3 reflectins in the tunable iridocytes. Results in prior Figure 36 show that these structures appear only when the reflectins are condensed, and Figure 35 shows that neutralization drives this condensation (as seen in the electron micrographs in Figure 34, and schematically in Figure 33).

Dynamic light scattering (DLS) confirms that these tunable changes are fully reversible and repeatedly cyclable. Using the purified, recombinant reflectins, and replacing the physiological charge-neutralizing "switch" of phosphorylation in the living biological system by convenient manipulation of pH [which we showed to be highly effective surrogate for phosphorylation, driving the structural transitions of the metastable recombinant reflectins *in vitro* (cf. Figures 34 and 35, above)], DLS analyses show the neutralization-dependent tunable assembly of the reflectins and its reversibility and cyclability, (Figure 38):

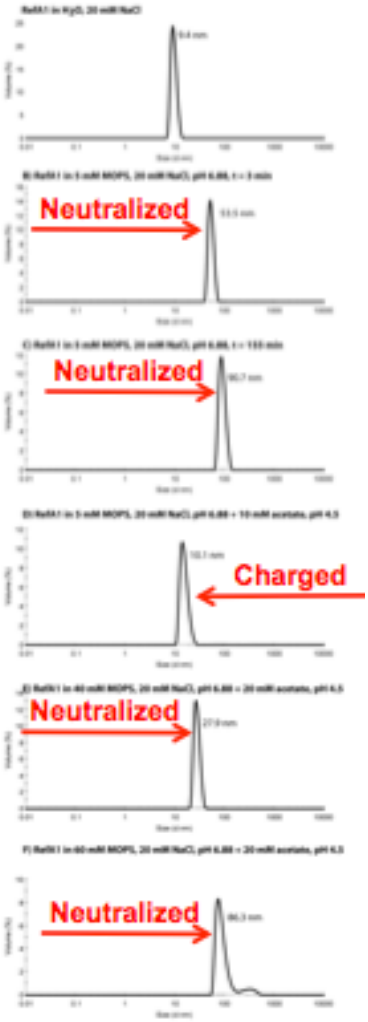

Figure 38: Dynamic Light Scattering shows progressive, reversible and cyclable changes in dimension as a function of time after neutralization, acidification, and re-neutralization. Starting from the monomer in acidic water at ca. 1-2 nm diameter (17), neutralization progressively drives assembly to the oligomer (ca. 10 nm) and higher-order multimer (ca. 90-100 nm). Re-acidification drives reversible dis-assembly back to the oligomer and smaller, while a second cycle of neutralization drives assembly.

Results in Figure 39 show that (a) metastability of the reflectins is poised with a hair trigger between the uncondensed and condensed states, and (b) neutralization of only 2-4 charges per molecule (corresponding to the addition of only one or two PO_4^{-2} groups) is needed to trigger the full conversion. This is one of the most subtle and most complex protein-mediated signal transduction systems yet discovered, and the first to be discovered that regulates a tunable biophotonic function without any chromophores! The colorless reflectin proteins mediate the tunability of color and intensity solely by controlling the reversible assembly, structure and dimensions of photonically active, tunable nanostructures – all as a result of their linear sequences encoded directly in the DNA of their genes! Most significantly, this discovery reveals the power and general applicability of metastability as a design principle for reconfigurable biological and new synthetic materials.

Our work on photonic camouflage in deep-sea squids also led us to consider the reflectin-like system in giant clams. This inquiry led to a remarkable discovery of a solar energy harvesting - full optical characterization of a system that will allow efficient harvesting of photons in a low surface area, damage-resistant system. This system consists of photosynthetically active dinoflagellates organized into micropillars within the clam's mantle tissue, and wavelength-dependent iridocyte scattering cells that interact with these pillars to redistribute photosynthetically efficient light evenly among cells and deep into the tissue. We characterized the clam system using micron-scale intra-tissue radiometry and optical modeling, and found that this multi-scale system results in a five-fold increase in light reaching dinoflagellates compared to the same number of cells organized in a simple layer (figure 40). The evolved photonic system in the clam may present new strategies for more efficient, damage-resistant polymer-based photovoltaic devices and sunlit, spatially efficient algal biofuel production. This work was published in 2014 (Holt et al., 2014).

Our work on reflectin-based tissue transcriptomes and characterization of the structures they make led in a completely unexpected direction with potentially significant implications for the field of self-assembly more generally. A thorough analysis of our mass spectroscopy data in concert with our transcriptome data has revealed that reflectin proteins are RNA edited at totally unprecedented rates, of about 2% of nucleotides in the full-length transcripts, and this editing is reflected in the protein content of the cells. The presence of the encoded proteins in our MS/MS pool confirms that this nucleotide polydispersity is present in the reflectin protein ensemble in the cell. We used graph theory to identify "editing cycles" of RNA sequences related by editing to parent DNA sequences. This approach revealed a number of parent sequences on order of the 5-10 major protein bands observed in SDS-PAGE preparations of these tissues. Polydispersity at small spatial scales has been posited by theorists to be important for initiating self-assembly processes; our observations in the evolved reflectin-based systems may provide an important test of theoretical predictions and source of new empirical insights into self-assembly at the nanoscale. Similarly, between-amino acid edits may give us new functional insights into reflectin function.

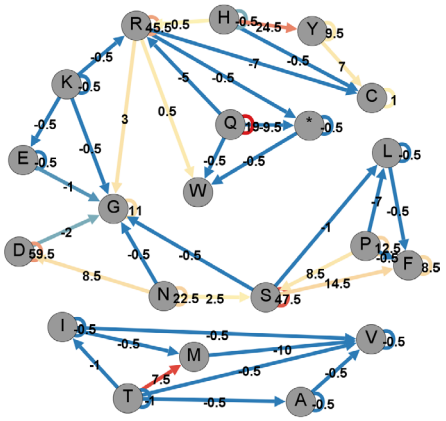

Figure 39. Between-amino acid RNA edit cycles of reflectin proteins. Edits to aliphatic residues are disfavored, while edits to and among aromatic and charged and disorder-inducing residues are favored.

Our finite-difference time domain model of *Galiteuthis* light guides revealed a novel physical mechanism for radiance-matching in the open ocean. The subocular photophores in this genus had previously been suggested to play a role in counter-illumination camouflage. This hypothesis assumes that only matching radiance in one downward direction to hide from predators looking directly upward is important to the visual ecology of these animals. Our work showed the counterintuitive result of "leaky" light guides. Intriguingly, there are a few cells in the animal that make quite efficient light guides, demonstrating that this inefficiency is purposeful and isn't simply a limitation of biological organization or complexity. The most common cells in the photophore organ, however, are the leaky, or less efficient light guides. When we compared the radiance emitted from single light-guiding cells in the subocular photophore, we found that it was a surprisingly good match to the predicted radiance in the ocean (Figure 41). Further, the numerous less-efficient cells provide a good radiance match to shallow depths in the animals' vertical range where there is more light and relatively more horizontal radiance compared to downwelling radiance. The less frequent but more efficient cells provide a good radiance match to deeper depths in the animals' vertical range where there is less light and relatively more of it is downwelling. To our knowledge, this result is the first detailed physical mechanism described for dynamically matching ocean radiance throughout the water column.

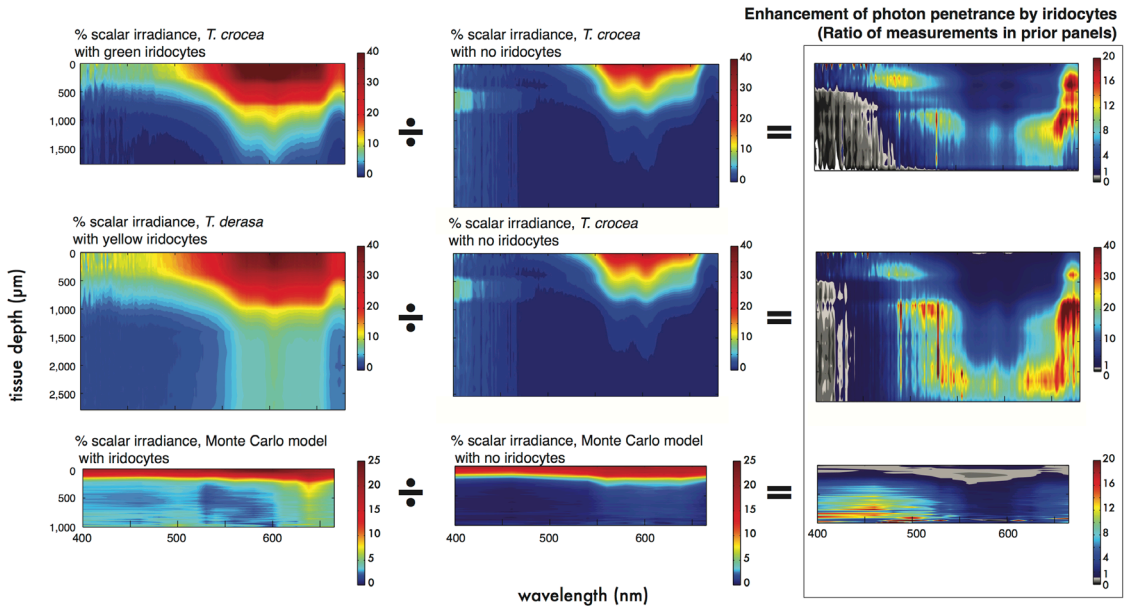

Figure 40. Optical performance of giant clams with and without iridocytes, and a Monte Carlo optical model recapitulating this performance, showing enhanced scalar irradiance.

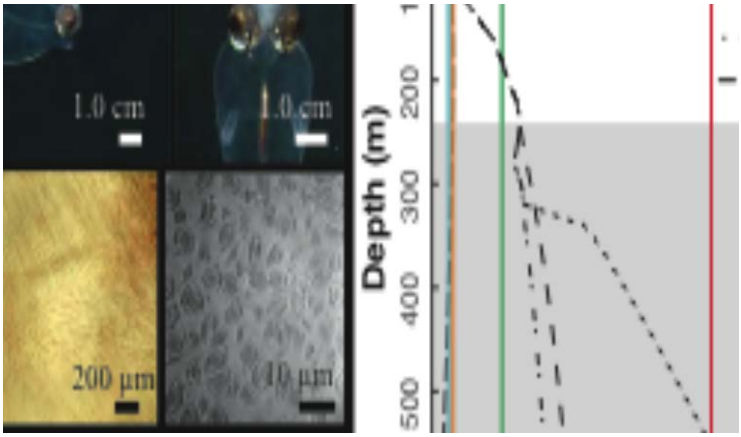

Figure 41: Left panel: **Galiteuthis** ***and orientation of light-guiding cells in the sub-ocular photophore. Right panel: Light-guiding fibers vary in their transmission efficiency. The most common fibers in the eye are actually the least efficient. The radiance of inefficient fibers matches ocean radiance at shallow depths, suggesting that the fibers are a radiance-matched solution to open water camouflage***

Our investigations of the peculiar scale structure in hatchetfish, both experimentally through BRDF, and through modeling, reveal an interesting scattering anisotropy (Figure 42). Beams directed toward the fish's flanks are preferentially scattered into a plane orthogonal to the dorsoventral axis of the animal. We showed using finite-difference time domain modeling how this scattering emerges from the sub-wavelength structure of the unusual scales of the hatchetfish. This scattering mechanism may provide some camouflage for hiding against predators with bioluminescent searchlights, ensuring that the beam is both deflected away from the source, diffused such that the reflected beam itself is also not visible in the water column, and is not visible scattering within or on the body of the animal.

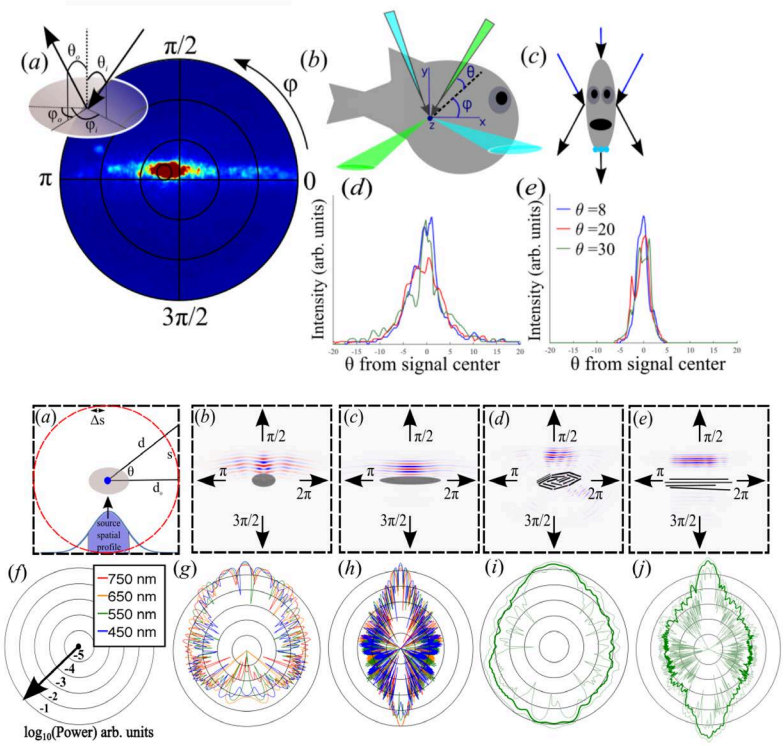

Figure 42: Left panel: Finite difference time domain modeling of hatchetfish skin. The subwavelength structure of the scales, combined with their long axes orthogonal to the section shown here act together to scatter light into a plane orthogonal to the animal's body. We outline a mechanism by which this might provide a mechanism for hiding from bioluminescent searchlights, akin to last-generation stealth radar camouflage.

We have also initiated a study of the long-wavelength reflecting structures present in squid skin (such as in *Loligo opalescens*, *Chiroteuthis dux*, *Pterygioteuthis lampas*, and *Dosidicus gigas*). Our initial models suggest that the predominantly long-wave (600 – 700 nm) reflectance of these structures may provide good camouflage against Raman-scattered light and photons from chlorophyll fluorescence in the ocean.

IMPACT/APPLICATIONS

The systems evolved by marine animals in order to hunt, hide, and mate over hundreds of million years surpass our contemporary engineering designs for underwater vehicles. Hiding and hunting are natural tasks for our military and we believe that valuable clues will be provided by the results of our studies. The impact will hopefully affect all branches of the armed forces that have aquatic missions. This includes Special Forces, mine hunting vehicles, the submarine community, and a newest generation of underwater vehicles that could all benefit from the option of "stealth". Since visual methods play an important role in the mission profiles of all of these groups, the ability to enhance and hide from detection should be an important payoff.

The discoveries reported above point to simple new methods to achieve effective camouflage for moving objects and effective edge disruption in shallow-water and caustic day-time light environments. We have been working in close collaboration with partners at Raytheon Vision Systems Inc. since the start of this project, seeking to develop practical translations of the signature management and other useful technologies, materials and devices important to industry, the Navy and other units of DoD. Our focus is to develop low-power electrically switchable polymer-based materials for these purposes. Through this collaboration we have developed a prototype biologically inspired, lightweight, electrically switchable, polymer-based shutter for IR detectors that can be extended to coded apertures for IR imaging without a lens and to signature management in the IR (cf. patent awarded last year). In addition, the giant clam system may suggest novel geometries for devices for solar energy harvesting.

TRANSLATIONS

(1) <u>Electrically switchable, polymer-based shutters for IR detectors</u>: As described in our report, we discovered the molecular structures and mechanisms responsible for the dynamically tunable reflectance in skin cells of the squid, and are now working with Raytheon Vision Systems Inc. (with support from ARL and DARPA) to translate these finding to develop a prototype electrically switchable, polymer-based shutter for infrared detectors. Using solution-processable conjugated polymers, we developed working prototypes that are activated by low voltage (2-3 V) to display significant changes in absorption and reflection in the IR. As the polymer-based materials transition from semiconducting to conducting, free carriers and conformational changes absorb and scatter broad bands of infrared radiation. The resulting change in refractive index resulting from the simultaneous production of absorbing species and their increased density closely parallels the synergistic simultaneous changes in the reflectin-based Bragg layers that provide the high gain exhibited by the biological system. Defense applications include noiseless IR shutters for forward Special Forces operations, graded neutral density and tunable hyperspectral IR filters, apertures, and lightweight coded apertures for IR image formation without a lens.

(2) <u>Broadband, omnidirectional IR reflectors</u>: Also as described above, we recently discovered that the silver, broadband reflective tissue surrounding the eyes of the squid (providing omnidirectional camouflage of that structure) is composed of a unique array of reflectin-filled, spindle-shaped cells densely packed together to form an unusual, quasi-disordered, "distributed Bragg reflector." The optical contrast between the high refractive index within these reflectin-packed cells and the low refractive index in the extracellular medium is responsible for the very high reflectivity of the tissue, while the infinite number of spacings between the nested, tapered cells in the quasi-disordered array is responsible for the broadband (i.e., multi-wavelength, silver) and omnidirectional reflection. Translating the underlying principles found in this biological broadband reflector (in research supported by ARO and Acumen, Inc.), we produced prototype broadband reflective coatings by evaporative self-assembly of asymmetric polymer rods to form quasi-disordered and "distributed" Bragg reflectors. The dimensions of the quasi-ordered polystyrene rods are sufficiently large to ensure that reflectance occurs in the IR, while the random quasi-disorder of the film ensures omnidirectionality of the reflectance. Silica and silicone casts of these organic films retain the optical properties in a rugged form suitable for device manufacture. Because the biologically inspired fabrication process is facile, error-tolerant and inexpensive and can be scaled to larger, flexible and curved surfaces; because silica and silicone casts preserve the desired optical features in a robust form suitable for manufacture of coatings; and because the optical and IR properties of those coating can be

readily tuned, they offer numerous applications of potential importance to ONR and other branches of DoD.

RELATED PROJECTS

"Bioinspired Dynamically Tunable Polymer-Based Filters for Multi-Spectral Infrared Imaging"; DARPA; W911NF-08-1-0494; $150,000; 10-01/08-09/30/09. To D. E. Morse. This work represents a "translation" of what we learned from the biomolecular mechanisms governing dynamically tunable reflectance in cephalopods to novel routes for synthetic optical materials. Performed in collaboration with Raytheon, Inc. This funding has ended; proposal for continuation is pending.

“Bio-inspired Visual Information Processing and Dynamically Tunable Multispectral IR Detection: Learning from the Octopus.” ARL/ARO; W911NF-09-D-0001; $200,000; 1/1/09-12/31/09. To D.E. Morse and R. N. Hanlon. This work represents a "translation" of what we learned from the biomolecular mechanisms governing dynamically tunable reflectance in cephalopods to novel routes for synthetic optical materials. This funding has ended.

”Bio-Inspired Photonics: Polymer-Based, Dynamically Tunable Multi-Spectral Filters for IR Detection”; DARPA; proposal by D. E. Morse pending for continuation of effort described immediately above. This work represents a "translation" of what we learned from the biomolecular mechanisms governing dynamically tunable reflectance in cephalopods to novel routes for synthetic optical materials.

PUBLICATIONS (37 in print or press, 5 in review, 11 in prep)

Akre, K. L. and Johnsen, S. (2014). Psychophysics and the evolution of behavior. *Trends in Ecology and Evolution* **29**, 291-300.

Akre, K. L., and S. Johnsen (in review). Communication through a window of error: Proportional processing and signal categorization. In *Perception and Cognition in Animal Communication*, (Bee M. A., Miller, C. T., eds.), Springer.

Akre, K. L., Ryan, M. J., and S. Johnsen (in prep). Elaborately redundant female sexual signaling in brief squid (*Lolliguncula brevis*).

Bedore, C. N., Kajiura, S. M., and S. Johnsen (in review) Bioelectric crypsis in the cuttlefish *Sepia officinalis* reduces predation risk from electrosensitive predators. *Proceedings of the Royal Society of London: Biological Sciences*.

Bedore, C. N., Johnsen, S., and B. M. Williams (in prep). Tetrodotoxin the tissues of three cuttlefish species: *Sepia bandensis, Sepia officinalis, and Metasepia pfefferi*.

Bedore, C. N., Johnsen, S. and S. N. Patek (in prep). Comparative function of a ballistic-style feeding mechanism in two species of cuttlefish.

Brandley, N. C., Speiser, D. I., and S. Johnsen (2013). Eavesdropping on visual secrets. *Evolutionary Ecology.* **6**, 1045-1068.

DeMartini, D. G., M. Izumi, A. T. Weaver, E. Pandolfi and D.E. Morse. 2015. Structures, organization and function of reflectin proteins in dynamically tunable reflective cells *J. Biol. Chem.* doi/10.1074/jbc.M115.638254

DeMartini, D.G., A. Ghoshal, E. Eck and D.E. Morse (in prep). Discovery of tunable leucocytes, and a unified mechanism governing tunable biophotonics in squid.

DeMartini, D.G., A. Ghoshal, E. Pandolfi, A.T. Weaver, M. Baum, and D.E. Morse. 2013. Dynamic Biophotonics: Female Squid Exhibit Sexually Dimorphic Tunable Leucophores and Iridocytes. *J. Exp. Biol.* **216**, 3733-3741.

DeMartini, D.V. Krogstad and D. E. Morse. 2013. Membrane invaginations facilitate reversible water flux driving tunable iridescence in a dynamic biophotonic system. *Proc. Natl. Acad. Sci. USA* **110**, 2552-2556

Gagnon, Y. L., Sutton, T. T., and S. Johnsen (2013). Visual acuity in pelagic fishes and mollusks. *Vision Research* **92**, 1-9.

Gagnon, Y. L., Speiser, D. I., and S. Johnsen (2014). Simplifying numerical ray-tracing for characterizing imaging systems. *Applied Optics* **21**, 4784-4790.

Gassmann, E., Stramski, D., Darecki, M., and Dubranna, J. (in prep). Power spectra of wave-induced fluctuations in downward irradiance within the near-surface ocean under sunny conditions.

Gassmann, E., Stramski, D., Reynolds, R. A., and Johnsen, S. (in prep). Field measurements and radiative transfer simulations of the asymmetry of horizontal radiance within the upper ocean.

Ghoshal, A., D. G. DeMartini, E. Eck, and D.E. Morse (2013). Optical Parameters of the Tunable Bragg Reflectors in Squid. *J. R. Soc. Interface* **10**, DOI: 10.1098/rsif.2013.0386.

Ghoshal, A. D.G. DeMartini, E. Eck and D. E. Morse. 2014. Experimental determination of refractive index of condensed reflectins in squid iridocytes. *J. R. Soc. Interface* **11**, 20140106.

Haag, J. M., Jaffe, J. S., and Sweeney, A. M. (2013). Measurement system for marine animal reflectance functions. *Optics Express* **21(3)**, 3603-3616.

Haag, J. M., Jaffe, J. S. (in prep). BRDFs of deep sea creatures: Measurements and models.

Haag, J. M., Sweeney, A. M., and Jaffe, J. S. (2012). Measurement system for obtaining marine animal reflectance functions. *Proceedings of Ocean Optics XXI Conference*, Glasgow, Scotland, United Kingdom, October 8-12, 2012.

Haag, J. M., Roberts, P. L. D., Papen, G. C., Jaffe, J. S., Li, L., and Stramski, D. (2104). Deep-sea low-light radiometer system. *Optics Express* **22**, 30074-30091, DOI:10.1364/OE.22.030074.

Holt, A.L., Wehner, J.G.A., Hampp, A., and Morse, D.E. (2010). Plastic transmissive infrared electrochromic devices. *Macromolecular Chemistry and Physics* **211**, 1701-1707.

Holt, A.L.., Sweeney, A.M., Johnsen, S., and Morse, D.E. (2011). A highly-distributed Bragg stack with unique geometry provides effective camouflage for Loligo squid eyes. *Journal of the Royal Society: Interface* **8,** 1386-1399.

Holt, A.L., S. Vahidinia, Y. Gagnon, D. E. Morse and A. M. Sweeney. 2014. Photosymbiotic giant clams are transformers of solar flux. *J. R. Soc. Interface* **11,** 20140678.

Izumi, M., A. M. Sweeney, D. G. DeMartini, J. C. Weaver, M. L. Powers, A.R. Tao, T. V. Silvas, R. M. Kramer, W. J. Crookes-Goodson, L. M. Mäthger, R. R. Naik, R. T. Hanlon and Morse, D. E. (2010). Changes in reflectin protein phosphorylation are associated with dynamic iridescence in squid. *Journal of the Royal Society: Interface* **7**: 549-560.

Jaffe, J. S., Simonet, F. and B. Laxton. (2011), Omni-Cam: An autonomous free-descent omni-directional camera for measuring radiance in marine environments". Proc. IEEE Oceans Conf., Santander, Spain June 6-9.

Jaffe, J. S., Laxton, B., Zylinski, S. (2011). The Sub Sea Holodeck: Systems a system for simulating underwater optical environments in the lab. Proc. IEEE Oceans Conf., Santander, Spain June 6-9, 2011.

Johnsen, S., Marshall, N. J., and Widder, E. A. (2011). Polarization sensitivity as a contrast enhancer in pelagic predators: Lessons from *in situ* polarization imaging of transparent zooplankton. *Philosophical Transactions of the Royal Society of London, Series B*. **366**: 655–670.

Johnsen, S., Gassmann, E., Reynolds, R. A., Stramski, D., and Mobley, C. D. (2014). The asymmetry of the underwater horizontal light field and its implications for the mirror-based camouflage in silvery pelagic fish. *Limnology and Oceanography*, **59**, 1839-1852.

Johnsen, S., Gagnon, Y., Marshall, N. J., Cronin, T. W., Gruev, V., and S. Powell (in prep: accepted for review at *Current Biology*). Polarization vision does not break the mirror-based camouflage of silvery fish.

Johnsen, S. (2014). Hide and seek in the open sea: Pelagic camouflage and visual countermeasures. *Annual Review of Marine Science* **6**, 369-392.

Li, L., Stramski, D., and Reynolds, R. A. (2014). Characterization of the solar light field within the ocean mesopelagic zone based on radiative transfer simulations. *Deep-Sea Research I,* **87**, 53-69.

Levenson, R. N. Bush, C. Bracken and D.E. Morse. (in review). Cyclable condensation and hierarchical assembly of metastable reflectin proteins, the drivers of tunable biophotonics. *J. Biol. Chem.*

Li, Z., Zhang, Y., Holt, A.L., Kolasa, B.P., Wehner, J.G., Hampp, A., Bazan, B.C., Nguyen, T., and Morse, D.E. Electrochromic devices and thin film transistors from a new family of ethylenedioxythiophene based conjugated polymers. *New Journal of Chemistry* **35**: 1327-1334.

Marshall, N. J., and Johnsen, S. (2011). Camouflage in Marine fish. In *Animal Camouflage: Current issues and new perspectives*. Cambridge University Press: Cambridge UK.

Nilsson, D. E., Warrant, E. J., Johnsen, S., Hanlon, R. T., and N. Shashar (2012). A unique advantage for giant eyes in giant squid. *Current Biology* **22**, 683-688.

Nilsson, D. E., Warrant, E. J., Johnsen, S., Hanlon, R. T., and N. Shashar (2013). The giant eyes of giant squid are indeed unexpectedly large, but not if used for spotting sperm whales. *BMC Evolutionary Ecology* **13**, 187-189.

Nilsson, D. E., Warrant, E. J., and S. Johnsen (2014). Computational visual ecology in the pelagic realm. *Philosophical Transactions of the Royal Society of London, Series B* **369**, 20140038.

Orenstein, E. C., Haag, J. M., Gagnon, Y. L., and J. S. Jaffe (in review). Automated classification of camouflaging cuttlefish. *Methods in Oceanography, special issue on Computer Vision in Oceanography*.

Sawicka, E., Stramski, D., Darecki, M., and Dubranna, J. (2012). Power spectral analysis of wave-induced fluctuations in downward irradiance within the near-surface ocean under sunny conditions. *Ocean Optics XXI*, Glasgow, Scotland. Program & Abstracts, p. 133-134.

Sweeney, A., Johnsen, S., A. Holt and D.E. Morse (in prep). Natural camouflage in the infrared? Predators and prey in the ocean's far-red Raman glow.

Sweeney, A.M., G. E. Clague, M. Baum, D.G. DeMartini, and D.E. Morse (in prep). Discovery of a reflectin-transglutaminase fusion protein in photonic cephalopod tissues.

Taniguchi, D. A. A., Gagnon, Y., Wheeler, B. J., Johnsen, S., and J. S. Jaffe (in press). Cuttlefish *Sepia officinalis* preferentially respond to bottom rather than side stimuli when not allowed adjacent to tank walls. *PLoS ONE.*

Tao, A.R., D. G. DeMartini, M. Izumi, A. M. Sweeney, and Morse, D. E. (2010). The role of protein assembly in dynamically tunable bio-optical tissues. *Biomaterials* **31**, 793-801.

Warrant, E. J., and S. Johnsen (2013). Vision and the light environment. *Current Biology* **23**, R990-R994.

Zylinski, S., and Osorio, D. (2011). What can camouflage tell us about non-human visual perception? A case study of the cuttlefish. In *Animal Camouflage: Current issues and new perspectives*. Cambridge University Press: Cambridge UK.

Zylinski, S. How, M., Osorio, D., Hanlon, R. T., and Marshall, N. J. (2011). To be seen or to hide: visual characteristics of body patterns for camouflage and communication in the Australian giant cuttlefish, *Sepia apama*. *American Naturalist* **177,** 681-690.

Zylinski, S. and S. Johnsen (2012) Camouflage without compromise: Mesopelagic cephalopods switch between transparency and pigmentation to optimize camouflage in the deep. *Current Biology* **21,** 1937-1941.

Zylinski, S., A.-S. Darmaillacq, & N. Shashar (2012). Visual interpolation for contour completion by the European cuttlefish (*Sepia officinalis*) and its use in dynamic camouflage. *Proceedings of the Royal Society B: Biological Sciences* **276**, 3963-3969.

Zylinski, S. and S. Johnsen (2014). Visual cognition in deep-sea cephalopods: what we don't know and why we don't know it. Pp. 223-243 in: *Cephalopod Cognition*, Editors: S. Darmaillacq and J. Mather. Cambridge University Press.

Zylinski, S. and D. Osorio (2014). Cuttlefish camouflage: Vision and cognition. Pp 197-222 in: *Cephalopod Cognition*, Editors: S. Darmaillacq and J. Mather. Cambridge University Press.

Zylinski, S., Gagnon, Y., Gross, T., Wheeler, J. and Johnsen, S. (in prep.). *Octopus bimaculoides* substrate choice: hierarchy and interactions between visual and tactile information.

Zylinski, S., Johnsen, S., and D. Osorio (in review). European cuttlefish *Sepia officinalis* fine-tunes camouflage using asymmetrical shading in response to pictorial depth cues and directional illumination. *Proceedings of the Royal Society of London: Biological Sciences*.